國立臺灣大學理學院物理學系

碩士論文

Department of Physics

College of Science

National Taiwan University

Master's Thesis

單缺陷非厄米系統與邊界共形場論

Single Impurity non-Hermitian System and Boundary Conformal Field Theory

陳柏豪

Bo-Hao Chen

指導教授: 謝長澤 博士

Advisor: Chang-Tse Hsieh Ph.D.

中華民國 114 年 6 月

June, 2025

doi:10.6342/NTU202501665

國立臺灣大學碩士學位論文
口試委員會審定書

MASTER'S THESIS ACCEPTANCE CERTIFICATE
NATIONAL TAIWAN UNIVERSITY

單缺陷非厄米系統與邊界共形場論

Single Impurity non-Hermitian System and Boundary Conformal Field Theory

本論文係陳柏豪（R11222054）在國立臺灣大學物理學系完成之碩士學位論文，於民國 114 年 6 月 4 日承下列考試委員審查通過及口試及格，特此證明。

The undersigned, appointed by the Department of Physics, National Taiwan University on 04 June 2025 have examined a Master's thesis entitled above presented by CHEN, BO-HAO (R11222054) candidate and hereby certify that it is worthy of acceptance.

口試委員 Oral examination committee:

謝長澤		伍祥華
（指導教授 Advisor）		
沈家賢		

doi:10.6342/NTU202501665

Acknowledgements

能夠完成這篇學位論文，首先我要感謝的是我的指導教授謝長澤老師，以及我的合作者姚有徽學長，若沒有他們，我的研究就無法順利完成。此外，我要感謝擔任口試委員的陳俊瑋老師、沈家賢老師以及任祥華老師。另外我要特別感謝物理系的的胡德邦老師、江正天老師、程之寧老師、楊超強老師，與他們的討論讓我受益良多。最後我要感謝我的朋友柏廷、友安、育維、樹德在這段時間對我的支持，以及我的父母在我就讀碩士期間的經濟支援。

doi:10.6342/NTU202501665

doi:10.6342/NTU202501665

摘要

共形場論對描述臨界現象中的普適性行為提供了一套精確的分析框架，而邊界共形場論則在理解臨界系統中的量子雜質問題方面扮演重要的角色。另一方面，非厄米物理源於放寬厄米性條件，能有效刻畫具有增益、耗散與衰減等現象的開放量子系統的動力學。受這些發展的啟發，我們探討非么正邊界共形場論與非厄米量子雜質臨界系統之間的關聯。我們將邊界共形場論的框架擴展至包含非厄米雜質的情況，並利用折疊技巧將晶格模型中的雜質強度對應到一個有效的位勢參數，從而建立晶格散射矩陣與邊界共形場論黏合矩陣之間的對應關係。在此對應中，非厄米模型中機率守恆的違反體現在邊界共形場論中非么正的邊界條件。我們進一步顯示，晶格模型在費米點所產生的雜質能量位移，與邊界共形場論中基態能量的有限尺寸修正相符；該修正隨系統尺寸呈反比縮放，並由費米動量下的傳輸振幅所決定。這項結果推廣了對厄米雜質系統的既有研究成果，例如 [1, 2] 中所提出的。總結而言，我們的研究表明，邊界共形場論的技術可以有效應用於非厄米量子雜質問題的分析，為非厄米性與邊界或缺陷臨界性之間的關係提供了新的見解。

關鍵字：共形場論、邊界共形場論、非厄米、缺陷、散射矩陣

doi:10.6342/NTU202501665

doi:10.6342/NTU202501665

Abstract

Conformal field theory (CFT) offers an exact analytical framework for describing the universal features of critical phenomena, while boundary conformal field theory (BCFT) plays a central role in understanding quantum impurity problems at criticality. Meanwhile, non-Hermitian physics, which arises from relaxing the Hermiticity condition, effectively captures the dynamics of open quantum systems with gain, loss, and decay. Motivated by these developments, we explore the connection between non-unitary BCFT and non-Hermitian quantum impurity critical systems. Extending the BCFT framework to include non-Hermitian impurities, we map the lattice impurity strength to an effective barrier parameter using the folding trick, establishing a direct correspondence between the lattice scattering matrix and the BCFT gluing matrix. In this correspondence, the violation of probability conservation in the non-Hermitian model manifests as non-unitary boundary conditions in BCFT. We further show that the impurity-induced energy shift at the Fermi point(s) in the lattice model matches the finite-size correction to the ground-state energy in

doi:10.6342/NTU202501665

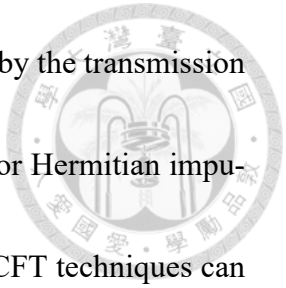

BCFT, which scales inversely with the system size and is determined by the transmission amplitude at the Fermi momentum. This extends the known results for Hermitian impurity systems, e.g., presented in [1, 2]. Our results demonstrate that BCFT techniques can be fruitfully applied to the study of non-Hermitian quantum impurity problems, providing new insights into the interplay between non-Hermiticity and boundary or defect criticality.

Keywords: Conformal Field Theory, Boundary Conformal Field Theory, non-Hermitian, Impurity, S-matrix

doi:10.6342/NTU202501665

Contents

doi:10.6342/NTU202501665

doi:10.6342/NTU202501665

doi:10.6342/NTU202501665

doi:10.6342/NTU202501665

List of Figures

doi:10.6342/NTU202501665

doi:10.6342/NTU202501665

List of Tables

doi:10.6342/NTU202501665

doi:10.6342/NTU202501665

Denotation

CFT	Conformal Field Theory
BCFT	Boundary Conformal Field Theory
c	central charge in BCFT
h	conformal dimension in BCFT
ℓ_n	Witt algebra generator
L_n	Virasoro algebra generator
$T(z)$	energy-momentum tensor
L	system size
H	Hamiltonian
$c_i^\dagger(c_i)$	creation (annihilation) operator
t_0	uniform hopping strength in tight binding model
$v(\bar{v})$	impurity strength

doi:10.6342/NTU202501665

$h.c.$	Hermitian conjugation
k	wave number (momentum)
$\psi_k(x)$	wave function
$\psi_k^{\pm}$	left (right) moving wave function in lattice system
S_k	scattering matrix
$T_k^{\pm}$	transmission amplitude
$R_k^{\pm}$	reflection amplitude
$_F$	the physical quantity at Fermi level
v_F	Fermi velocity
$\psi_{\text{in}}(\psi_{\text{out}})$	incoming (outgoing) wave function
U	gluing matrix in BCFT
$g, \bar{g}$	coupling strength in BCFT
σ^i	Pauli matrix
$\psi_R(\psi_L)$	right (left) moving fermionic field in BCFT
$X(Y)$	bosonic field in BCFT
$\|BD\rangle$	boundary state in BCFT
$\|ND\rangle(\|DD\rangle)$	Neumann (Dirichlet) boundary state in BCFT

doi:10.6342/NTU202501665

(σ, τ) or (s, t)	(spectral,time) direction in BCFT
$\lambda_{\pm}$	eigenvalues of scattering matrix
q_n	quasi momentum
$\phi_{\pm}$	phase shift due to impurity
ϕ_F	redefined phase shift strength
E_{GS}	ground state energy
$\tilde{c}_n$	coefficient of energy expansion in L^n order
E	energy in BCFT
E_0	ground state energy in BCFT
δ	phase shift due to boundary term in BCFT
E_N	particle-hole excitation energy
E_Q	excitation energy of additional Q particles
$n(m)$	excitation number of $X(Y)$ boson in BCFT
N	excitation number of bosonic field oscillation in BCFT

doi:10.6342/NTU202501665

doi:10.6342/NTU202501665

Chapter 1 Introduction

1.1 Motivation and Objectives

While things change with the passage of time and nothing appears eternal, physics offers a contrasting perspective: the existence of conserved quantities and scale-invariant structures suggests an underlying order. This is particularly compelling in the context of conformal field theory (CFT), where symmetries reveal deep, timeless patterns. In our study, we focus on the 1+1-dimensional case, where the richness of CFT is especially pronounced due to its infinite-dimensional symmetry algebra.

The language of field theory has a long-standing history in the description of condensed matter systems. The second quantization formalism, in particular, has played a central role in the development of key concepts such as the Fermi liquid paradigm. Field theory provides a rich set of well-developed formalisms and computational tools, which have been successfully adapted to describe lattice systems and to predict novel phenomena in condensed matter physics. This approach has led to numerous significant results.

Conformal Field Theory (CFT) offers an exact analytical framework for capturing the universal features of critical phenomena, particularly in two dimensions. In this setting, the theory benefits from an infinite-dimensional symmetry algebra, which enables exact

doi:10.6342/NTU202501665

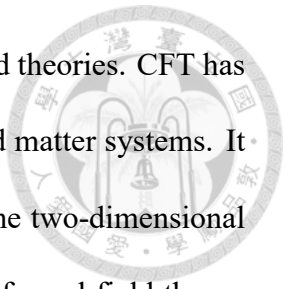

solutions that often lie beyond the reach of more general quantum field theories. CFT has been especially influential in the study of low-dimensional condensed matter systems. It has provided deep insights into scaling behavior in models such as the two-dimensional Ising model. Moreover, it serves as the foundation for boundary conformal field theory (BCFT), which is essential for understanding quantum impurity problems, including the Kondo effect and Luttinger liquid behavior.

On the other hand, non-Hermitian physics has seen rapid growth in recent years, driven by its broad range of applications. Non-Hermitian quantum mechanics, which emerges from relaxing the requirement of Hermiticity, effectively captures the dynamics of open systems, including phenomena such as gain, loss, and decay. Notably, PT-symmetric models can exhibit entirely real spectra and have been experimentally realized in various platforms, particularly in photonics. These developments have opened new avenues in both theoretical and applied physics.

Given that CFT can describe lattice systems and that BCFT is well-suited for modeling systems with defects or boundaries, it is natural to consider a correspondence between non-unitary BCFT and non-Hermitian systems. In this work, we extend the existing framework to incorporate non-Hermitian impurities by mapping the lattice impurity strength v to a complexified effective barrier parameter g. A non-Hermitian lattice system with a localized impurity is then mapped to a BCFT with a sine-Gordon boundary interaction via the folding trick, establishing a direct correspondence between the lattice scattering matrix and the BCFT gluing matrix. This mapping introduces non-unitarity into the scattering matrix, which manifests as nontrivial boundary conditions in the BCFT description. Specifically, Neumann boundary conditions in BCFT correspond to the disconnected or infinite barrier case in the lattice model, while Dirichlet boundary conditions correspond

doi:10.6342/NTU202501665

to a defect-free system. The impurity strength in the lattice model is identified with the boundary coupling in the BCFT. In this correspondence, Hermiticity of the lattice system translates to unitarity of the gluing matrix in BCFT. When Hermiticity (unitarity) is violated, the gluing and scattering matrices instead obey $SL(2,\mathbb{C})$ symmetry rather than $SU(2)$, reflecting the non-conservation of probability in the non-Hermitian system.

A key feature of this correspondence is that the impurity-induced energy shift at momentum $k = \pi/2$ in the lattice model matches the finite-size correction to the BCFT ground-state energy. Moreover, the correspondence extends to excited states: the L^{-1} corrections to excited-state energies are captured exactly. In this mapping, the excitation number N in BCFT corresponds to the total excitation energy in the lattice model arising from promoting the $i-th$ particle by N_i levels, effectively creating particle-hole pairs. Notably, we identify two distinct types of excitation numbers with physical significance. The charge-like excitation number, defined as the total number of excess particles in the left- and right-moving sectors, maps onto excitation modes of the decoupled Y-boson sector. In contrast, the chiral-like excitation number, given by the difference in particle numbers between these sectors, corresponds to excitations in the interacting X-boson sector. This distinction reveals an intriguing separation between charge and chiral modes in the system. Additionally, we find that the ground-state degeneracy under periodic boundary conditions, as well as the shift between integer and half-integer excitations under periodic versus anti-periodic boundary conditions, reflecting the underlying conformal tower structure encoded in the BCFT.

This mapping provides a unified framework for describing open quantum systems with gain and loss in terms of conformal boundary data. It enables the application of BCFT techniques to analyze non-Hermitian critical behavior, offering new insights into

doi:10.6342/NTU202501665

impurity physics and non-Hermitian phenomena in condensed matter systems.

1.2 Overview of Thesis Structure

Chapter 2 provides an overview of prior work on non-Hermitian systems, covering both theoretical and experimental developments. For a comprehensive review, see Ref. [3].

Chapter 3 is divided into two parts. The first introduces conformal field theory and boundary conformal field theory, following standard textbook treatments as presented in [4–6]. The second part focuses on the boundary sine-Gordon model, originally studied in [7, 8] and later extended to the non-unitary regime in [9], which serves as the foundation for our analysis of the non-Hermitian BCFT correspondence.

Chapter 4 presents the main contributions of this thesis. Building on the perspective of [1, 2], we extend the analysis of impurity models to a broader class of non-Hermitian systems using the S-matrix formalism. We compute the scattering matrix and ground-state (critical) energy of the non-Hermitian system, and compare the results to those of the boundary sine-Gordon model introduced in Chapter 3. Employing the folding trick, we construct a correspondence between our model and the BCFT framework, elucidating features such as the boundary S-matrix, boundary conditions, and critical energy. We also discuss the physical implications and interpretative insights of this correspondence.

Chapter 5 summarizes the main findings and outlines potential directions for future research.

doi:10.6342/NTU202501665

Chapter 2 Non-Hermitian Physics

Conventional quantum mechanics is built upon Hermitian Hamiltonians, whose real eigenvalues ensure unitary time evolution and probability conservation in isolated systems. Relaxing the Hermiticity constraint to allow complex, non-self-adjoint operators gives rise to non-Hermitian Hamiltonians, which naturally describe processes such as energy exchange with the environment, radiative decay, and gain/loss dynamics in open systems [3]. A seminal result by Bender and Boettcher showed that a broad class of non-Hermitian Hamiltonians possessing combined parity–time (PT) symmetry can nevertheless exhibit entirely real spectra in the so-called unbroken phase, thereby extending the formal boundaries of quantum theory [10, 11].

Experimentally, such as photonics has emerged as a platform for exploring non-Hermitian phenomena, due to the precise control it offers over optical gain and loss. Also, exceptional-point (EP) physics has proliferated across diverse platforms, including photonics, acoustics, and electronics. Today, effective non-Hermitian Hamiltonians appear across a broad range of physical contexts, from nuclear and atomic decay, circuit dynamics, and active mechanical lattices [3]. In this chapter, we present a concise overview of the fundamental properties of non-Hermitian systems, highlight key experimental realizations, and outline major challenges that continue to drive ongoing research.

doi:10.6342/NTU202501665

2.1 Theoretical Background

2.1.1 Non-Hermitian Quantum Mechanics

In conventional quantum mechanics, the Hamiltonian operator H is required to be Hermitian ($H^\dagger = H$) to ensure that its eigenvalues are real and that the time-evolution operator $U(t) = e^{-iHt/\hbar}$ is unitary. Unitarity guarantees the conservation of probability, consistent with the optical theorem. However, in open systems, an effective description often involves a non-Hermitian Hamiltonian [3, 11].

Consider, for example, the non-Hermitian matrix:

$$M = \begin{pmatrix} 1 & i \\ i & 1 \end{pmatrix} \tag{2.1}$$

its Hermitian conjugate is

$$M^\dagger = \begin{pmatrix} 1 & -i \\ -i & 1 \end{pmatrix} \neq M \tag{2.2}$$

demonstrating that M is non-Hermitian. Consequently, its eigenvalues can be complex. To illustrate this, consider the following identity:

$$\lambda - \lambda^* = \frac{\mathbf{v}^\dagger M \mathbf{v}}{\mathbf{v}^\dagger \mathbf{v}} - \frac{\mathbf{v}^\dagger M^\dagger \mathbf{v}}{\mathbf{v}^\dagger \mathbf{v}} = \frac{\mathbf{v}^\dagger (M^\dagger - M) \mathbf{v}}{\mathbf{v}^\dagger \mathbf{v}} \neq 0 \tag{2.3}$$

which shows that a non-Hermitian operator may yield complex eigenvalues.

We can confirm this explicitly by solving for the eigenvalues and eigenvectors of the

doi:10.6342/NTU202501665

non-Hermitian matrix M. The results are:

$$\lambda_{\pm} = 1 \pm i, \quad v_{\pm} = \begin{pmatrix} 1 \\ \\ \pm 1 \end{pmatrix} \tag{2.4}$$

demonstrating that M possesses complex eigenvalues and associated eigenvectors, as expected for a non-Hermitian system.

Consider the general eigenvalue equation:

$$H\psi = E\psi \tag{2.5}$$

In non-Hermitian systems, the eigenvalues E can be complex, leading to complex energy spectra $E(k)$. The imaginary part of E encodes decay or amplification rates, reflecting the non-conservation of probability.

In the Schrödinger picture, the time evolution of a state vector is given by:

$$|\psi(t)\rangle = U(t)|\psi(0)\rangle = e^{-iHt/\hbar}|\psi(0)\rangle = e^{-iEt/\hbar}|\psi(0)\rangle \tag{2.6}$$

When $E \in \mathbb{C}$, the imaginary component governs exponential decay or growth of the wavefunction norm, corresponding to dissipative or amplifying behavior.

In conventional quantum mechanics, eigenvectors corresponding to distinct eigenvalues are orthogonal. However, in non-Hermitian systems, this orthogonality no longer holds. Consider two distinct right eigenvectors $\mathbf{v}_1 \neq \mathbf{v}_2$ of a non-Hermitian matrix M, with eigenvalues λ_1, λ_2, respectively. We find:

$$\lambda_2 \mathbf{v}_1^{\dagger}\mathbf{v}_2 = \mathbf{v}_1^{\dagger} M \mathbf{v}_2 = (M\mathbf{v}_1)^{\dagger}\mathbf{v}_2 = \lambda_1^{*}\mathbf{v}_1^{\dagger}\mathbf{v}_2 \tag{2.7}$$

doi:10.6342/NTU202501665

which leads to

$$(\lambda_1 - \lambda_2)\mathbf{v}_1^\dagger \mathbf{v}_2 \neq 0 \tag{2.8}$$

Therefore, unless $\lambda_1 = \lambda_2$, the inner product $\mathbf{v}_1^\dagger \mathbf{v}_2$ is generally non-zero, violating the orthogonality condition.

To resolve this, we introduce the concept of bi-orthogonality. For a non-Hermitian matrix M, we define right eigenvectors $\mathbf{v}_R$ and left eigenvectors $\mathbf{v}_L$, satisfying:

$$M\mathbf{v}_R = \lambda_R \mathbf{v}_R, \quad M^\dagger \mathbf{v}_L = \lambda_L^* \mathbf{v}_L \tag{2.9}$$

These lead to the bi-orthogonal condition:

$$\mathbf{v}_L^\dagger M \mathbf{v}_R = (M^\dagger \mathbf{v}_L)^\dagger \mathbf{v}_R = \lambda_L \mathbf{v}_L^\dagger \mathbf{v}_R \tag{2.10}$$

$$(\lambda_L - \lambda_R)\mathbf{v}_L^\dagger \mathbf{v}_R = 0 \tag{2.11}$$

Hence, left and right eigenvectors corresponding to distinct eigenvalues are orthogonal in the bi-orthogonal sense [12].

This generalized framework becomes especially crucial near exceptional points, where eigenstates coalesce and standard Hermitian assumptions break down. Non-Hermitian quantum mechanics thus extends the conventional Hilbert-space formulation while retaining predictive power across a wide range of open and driven systems [3, 13].

2.1.2 PT-symmetry and Real Spectra

A landmark discovery by Bender and Boettcher [10] demonstrated that non-Hermitian Hamiltonians possessing parity–time (PT) symmetry can exhibit entirely real and positive

doi:10.6342/NTU202501665

spectra. These systems can be viewed as analytic continuations of conventional Hermitian quantum mechanics into complexified phase space. Within this framework, PT-symmetric quantum mechanics replaces the Hermiticity condition with space-time reflection symmetry, yielding complex Hamiltonians that nonetheless support real spectra, unitary time evolution, and positive-definite inner products. This provides a mathematically consistent extension of quantum theory [11].

In one dimension, the parity operator P acts as spatial reflection $x \to -x$, while the time-reversal operator T performs complex conjugation. PT symmetry therefore imposes the condition:

$$[H, PT] = 0 \tag{2.12}$$

PT symmetry can be understood as a specific form of pseudo-Hermiticity, which is defined by the relation:

$$M^\dagger = \eta M \eta^{-1} \tag{2.13}$$

where $\eta = \eta^\dagger$ is a Hermitian operator. When $\eta = \mathbb{I}$, this condition reduces to standard Hermiticity.

For PT-symmetric systems, it holds that:

$$(PT)H(PT)^{-1} = H \tag{2.14}$$

Since T acts as complex conjugation, this condition can be rewritten as:

$$PHP^{-1} = H^\dagger \tag{2.15}$$

which reveals that the parity operator P plays the role of the metric operator η. Thus, PT

doi:10.6342/NTU202501665

symmetry is a special case of pseudo-Hermiticity.

A linear operator with a complete bi-orthonormal eigenbasis and a discrete spectrum is pseudo-Hermitian if and only if its eigenvalues are either entirely real or occur in complex conjugate pairs with equal multiplicities.[14] Pseudo-Hermiticity generalizes PT symmetry and provides a unifying framework for understanding the reality of spectra in non-Hermitian systems. It also supports extended constructs such as pseudo-supersymmetric quantum mechanics. A non-Hermitian Hamiltonian with a complete bi-orthonormal basis possesses a real spectrum if and only if it is pseudo-Hermitian with respect to a positive-definite inner product [15, 16].

Non-Hermitian photonics offers a powerful platform for realizing and probing parity–time (PT) symmetric quantum theories, effectively bridging fundamental physics with technological innovation through precise engineering of optical gain and loss [17]. The interplay of PT symmetry and non-Hermitian dynamics enables unprecedented control over light propagation, particularly near exceptional points, where system behavior becomes highly sensitive to perturbations. These features open new avenues for manipulating optical responses and advancing next-generation photonic applications [18, 19].

2.1.3 Exceptional Points

A defining characteristic of non-Hermitian spectra is the presence of exceptional points (EP), parameter values at which not only eigenvalues but also their corresponding eigenvectors coalesce [18]. Mathematically, an EP is a point in the system's parameter space where the Hamiltonian becomes non-diagonalizable: its geometric multiplicity (the number of linearly independent eigenvectors) is strictly less than its algebraic multiplic-

doi:10.6342/NTU202501665

ity (the degeneracy of the eigenvalue). As such, EP are branch-point singularities of the spectrum in the complex parameter plane [3].

At an EP, the eigenvalue is said to be defective, and the Hamiltonian cannot be diagonalized. Instead, it can only be brought into Jordan canonical form. A simple illustrative example is:

$$M = \begin{pmatrix} 1 & 1 \\ 0 & 1 \end{pmatrix} \tag{2.16}$$

which has a single eigenvalue

$$\lambda = 1, \quad v = \begin{pmatrix} 1 \\ 0 \end{pmatrix} \tag{2.17}$$

Here, the algebraic multiplicity of $\lambda = 1$ is 2, but the geometric multiplicity is only 1, indicating that M is not diagonalizable. This matrix exemplifies a Jordan block, the canonical structure of a matrix at an exceptional point.

The unique properties of exceptional points have been harnessed in a variety of technologies, including ultrasensitive sensors, enhanced gyroscopes, and mode-selective lasers [18, 19]. Beyond applications, non-Hermitian topology, characterized by exceptional degeneracies and the breakdown of conventional bulk–boundary correspondence, has revealed novel phases and phenomena such as the non-Hermitian skin effect and non-Hermitian analogs of Fermi surfaces, with far-reaching implications for both classical and quantum dissipative systems [13]. An example is provided by non-Hermitian atomic mirrors, which exhibit exceptional points, Fermi arcs, and a geometry-dependent skin effect that goes beyond the predictions of non-Bloch band theory, illustrating the rich interplay between non-Hermiticity, topology, and long-range interactions [20].

doi:10.6342/NTU202501665

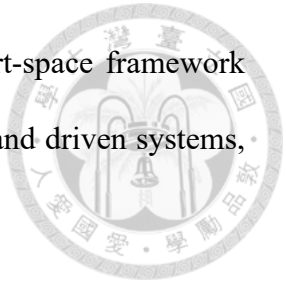

Overall, non-Hermitian quantum mechanics extends the Hilbert-space framework while preserving predictive power across a broad spectrum of open and driven systems, from nuclear resonances and atomic optics to photonic lattices [13].

2.2 Experimental Realizations and Applications

Photonics has emerged as a premier experimental platform for investigating non-Hermitian phenomena, owing to the fine-tuned control it affords over optical gain and loss. In coupled optical waveguides, the first direct observation of PT-symmetry breaking revealed non-reciprocal beam dynamics and power oscillations [21]. More recently, optical microcavities operated at exceptional points—spectral degeneracies where both eigenvalues and eigenvectors coalesce—have enabled ultrasensitive sensors whose response scales with the square root of perturbations, surpassing conventional detection limits [22]. Exceptional-point physics has since proliferated across a range of platforms, including photonics, acoustics, and electronics, as comprehensively reviewed in [18].

Beyond isolated spectral anomalies, non-Hermiticity fundamentally transforms band topology. Gong et al. proposed a periodic-table classification of complex-energy bands, revealing topological phases absent in Hermitian systems [23]. In such systems, even the bulk–boundary correspondence must be redefined: under open boundary conditions, bulk eigenstates can localize at a system's edge, giving rise to the non-Hermitian skin effect. This breakdown of conventional Bloch theory, along with the development of appropriate non-Bloch winding numbers, was elucidated by Yao and Wang [24] and has since been verified experimentally in mechanical meta-materials [25].

doi:10.6342/NTU202501665

2.3 Relation to non-unitary Conformal Field Theory

It is natural to seek connections between one-dimensional non-Hermitian quantum systems and (1+1)-dimensional non-unitary conformal field theories. Many exactly solvable (1+1)d CFT are non-unitary, yet they effectively describe critical behavior in one-dimensional quantum systems and two-dimensional statistical models through their rich symmetry structures and universal data [3].

Recent studies have extended key quantum information concepts to these non-unitary frameworks. For instance, entanglement entropy has been generalized to non-Hermitian systems using biorthogonal eigenstates and modified trace operations, revealing meaningful scaling behavior and enabling the definition of an effective central charge to characterize criticality in non-unitary CFT [26]. Furthermore, using biorthogonal bases, entanglement measures in non-Hermitian systems can capture topological features and critical behavior. A notable example is the PT-symmetric SSH model, which realizes a non-unitary CFT with central charge $c = -2$ [27].

From a topological perspective, Galois-conjugated non-unitary topological phases exhibit generalized topological protection but cannot be realized as ground states of Hermitian, gapped, local Hamiltonians. This rules them out as physically admissible phases in systems such as the fractional quantum Hall effect [28]. However, non-unitary string-net projected entangled pair states, constructed from Galois-conjugated fusion categories, do realize topological ground states of gapped non-Hermitian Hamiltonians. These include the Yang-Lee edge theory and other non-unitary topological sectors [29].

doi:10.6342/NTU202501665

2.4 Challenges and Open Questions

Despite significant progress, several key challenges remain. These include formulating unified dynamical bulk–boundary correspondence principles, mitigating noise amplification near higher-order exceptional points, and harnessing non-Hermitian topology to develop robust quantum and classical devices. Addressing these challenges promises not only to deepen our fundamental understanding of open-system quantum dynamics, but also to enable transformative technologies in sensing, lasing, and wave control [3].

doi:10.6342/NTU202501665

Chapter 3 Conformal Field Theory Techniques

Conformal field theory (CFT) has become a cornerstone of theoretical physics, particularly in the study of systems at criticality, where scale invariance governs physical behavior, and provides a powerful analytical framework for uncovering universal features of phase transitions and critical phenomena in both classical and quantum contexts. In two-dimensional systems, the infinite-dimensional nature of the conformal symmetry algebra enables exact solutions that are generally inaccessible in broader quantum field theory [4–6].

CFT has found wide-ranging applications in low-dimensional condensed matter systems, offering profound insights into universal scaling behavior. Notable examples include the two-dimensional Ising model [30, 31], and the analysis in fractional quantum Hall systems [32, 33]. Moreover, CFT serves as the theoretical foundation for Boundary Conformal Field Theory (BCFT), which has proven essential in describing quantum impurity problems such as the Kondo effect [34–38] and Luttinger liquids [39, 40].

This chapter introduces the fundamental structure and principles of Conformal Field Theory (CFT), including its symmetry content, operator formalism, and correlation functions, along with a brief overview of boundary conformal field theory (BCFT). These core

doi:10.6342/NTU202501665

concepts provide the foundation for subsequent discussions on BCFT, boundary scattering, and the application of conformal techniques to non-Hermitian defect systems.

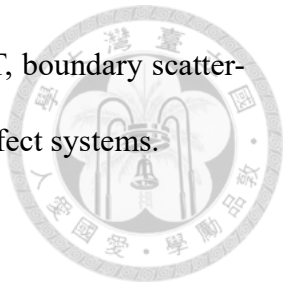

3.1 Brief introduction of CFT

3.1.1 Definition of Conformal Transformations

Conformal transformations are coordinate transformations that preserve local angles between vectors while allowing for position-dependent rescaling of lengths. Mathematically, a transformation $x^\mu \to x'^\mu(x) = x^\mu + \xi^\mu(x)$ is said to be conformal if it rescales the metric tensor by a local, smooth, positive function $\Omega(x)$:

$$g'_{\mu\nu}(x') = \Omega^2(x) g_{\mu\nu}(x) \tag{3.1}$$

This condition ensures that the causal and angular structure of spacetime is preserved, even though lengths may change locally.

In spacetime dimensions $d > 2$, the group of conformal transformations is finite-dimensional. It consists of the following generators: translations P_μ, rotations / Lorentz transformations $M_{\mu\nu}$, dilations D, and special conformal transformations K_μ. These generators close under commutation to form the conformal algebra $\mathfrak{so}(d, 2)$, which is isomorphic to the Lie algebra of the conformal group in d-dimensional Minkowski space. The total number of independent generators is given by

$$\frac{1}{2}(d+1)(d+2),$$

which exceeds the number of Poincaré generators by $d+1$, corresponding to the addition

doi:10.6342/NTU202501665

of dilations and special conformal transformations.

In two dimensions ($d = 2$), the structure of conformal symmetry becomes exceptionally rich. By introducing complex coordinates,

$$z = x + iy, \quad \bar{z} = x - iy \tag{3.2}$$

conformal transformations can be expressed locally as arbitrary analytic reparameterizations:

$$z \mapsto f(z), \quad \bar{z} \mapsto \bar{f}(\bar{z}) \tag{3.3}$$

where $f(z)$ is a holomorphic function and $\bar{f}(\bar{z})$ is its anti-holomorphic counterpart. Unlike in higher dimensions, the freedom to choose arbitrary analytic functions makes the conformal group in two dimensions infinite-dimensional.

This infinite symmetry leads to a natural decomposition of the theory into two independent sectors: a holomorphic (left-moving) sector and an anti-holomorphic (right-moving) sector, each governed by its own set of symmetry generators. These are associated with the Witt algebra (or its central extension, the Virasoro algebra), which plays a central role in two-dimensional conformal field theory.

3.1.2 Witt Algebra and Virasoro Algebra

The infinitesimal generators of local conformal transformations in the holomorphic sector are given by

$$\ell_n = -z^{n+1}\partial_z, \quad n \in \mathbb{Z} \tag{3.4}$$

doi:10.6342/NTU202501665

which satisfy the Witt algebra:

$$[\ell_m, \ell_n] = (m-n)\ell_{m+n} \tag{3.5}$$

This is a classical, infinite-dimensional Lie algebra capturing the symmetry of analytic reparameterizations.

Upon quantization, anomalies may emerge due to ambiguities in the regularization and normal ordering of composite operators. This results in a central extension of the Witt algebra known as the Virasoro algebra:

$$[L_m, L_n] = (m-n)L_{m+n} + \frac{c}{12}(m^3 - m)\delta_{m+n,0} \tag{3.6}$$

where c is the central charge, a key parameter that characterizes the conformal field theory. The Virasoro algebra governs the quantum dynamics of energy-momentum tensor modes and imposes stringent constraints on the spectrum and representation theory of two-dimensional CFT. For further details on the structure of the Virasoro algebra, see Appendix A.

The central charge c emerges as an anomaly in the conservation of the conformal current, slightly breaking the symmetry. In physical systems, the central charge plays several critical roles. It quantifies the number of effective degrees of freedom in the theory. In two-dimensional statistical mechanics, c determines the universal finite-size scaling of the free energy, and hence characterizes universality classes of critical behavior.

The central charge appears explicitly in the operator product expansion (OPE) of the

doi:10.6342/NTU202501665

holomorphic component of the energy-momentum tensor:

$$T(z)T(w) = \frac{c/2}{(z-w)^4} + \frac{2T(w)}{(z-w)^2} + \frac{\partial T(w)}{z-w} + \cdots \tag{3.7}$$

highlighting its foundational role in the algebraic structure of the theory and its influence on correlation functions, modular properties, and representation theory.

The central object responsible for generating conformal transformations in a conformal field theory is the stress-energy tensor $T_{\mu\nu}$. In two dimensions, due to the complex coordinate structure, it decomposes into holomorphic and anti-holomorphic components:

$$T(z) \equiv T_{zz}, \quad \bar{T}(\bar{z}) \equiv T_{\bar{z}\bar{z}} \tag{3.8}$$

These components satisfy conservation and traceless conditions consistent with local conformal invariance:

$$\partial_{\bar{z}} T(z) = 0, \quad T^{\mu}_{\mu} = 0 \tag{3.9}$$

The conservation equation implies that $T(z)$ is holomorphic, and similarly $\bar{T}(\bar{z})$ is anti-holomorphic. The stress-energy tensor admits a Laurent expansion in terms of the Virasoro generators:

$$T(z) = \sum_{n\in\mathbb{Z}} \frac{L_n}{z^{n+2}}, \quad \bar{T}(\bar{z}) = \sum_{n\in\mathbb{Z}} \frac{\bar{L}_n}{\bar{z}^{n+2}} \tag{3.10}$$

where L_n and $\bar{L}_n$ satisfy the Virasoro algebra. The action of $T(z)$ on primary fields determines their conformal weights and encodes their transformation properties under local conformal transformations.

doi:10.6342/NTU202501665

3.1.3 Operator Product Expansion (OPE)

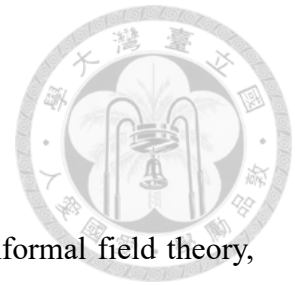

The operator product expansion (OPE) is a cornerstone of conformal field theory, encoding the short-distance behavior of local operators. When two fields are brought close together, their product can be expanded into a series of local operators:

$$\phi_i(z)\phi_j(w) = \sum_k C_{ijk}(z-w)^{h_k-h_i-h_j}\phi_k(w) + \cdots \tag{3.11}$$

where C_{ijk} are the OPE coefficients, and h_i, h_j, h_k are the conformal weights of the corresponding operators. This expansion is valid within correlation functions and captures the algebraic structure of the theory.

A particularly important case is the OPE between the holomorphic component of the stress-energy tensor $T(z)$ and a primary field $\phi(w)$ of conformal weight h:

$$T(z)\phi(w) = \frac{h}{(z-w)^2}\phi(w) + \frac{1}{z-w}\partial_w\phi(w) + \cdots \tag{3.12}$$

This OPE governs how primary operators transform under infinitesimal conformal transformations and encodes their representation under the Virasoro algebra. It also plays a central role in deriving Ward identities and computing correlation functions in 2D CFT.

Conformal symmetry imposes stringent constraints on the form of correlation functions involving primary operators. In two dimensions, the symmetry is powerful enough to completely fix the form of two-point and three-point functions up to constant coefficients.

The two-point function of primary fields $\phi_i(z_i, \bar{z}_i)$ takes the form:

$$\langle \phi_i(z_1, \bar{z}_1)\phi_j(z_2, \bar{z}_2)\rangle = \delta_{ij}\frac{1}{(z_{12})^{2h_i}(\bar{z}_{12})^{2\bar{h}_i}} \tag{3.13}$$

doi:10.6342/NTU202501665

where $z_{12} = z_1 - z_2$ and $\bar{z}_{12} = \bar{z}_1 - \bar{z}_2$. The Kronecker delta δ_{ij} ensures orthogonality between distinct conformal families.

The three-point function of primary fields is similarly fixed by conformal symmetry, for holomorphic part:

$$\langle \phi_1(z_1)\phi_2(z_2)\phi_3(z_3)\rangle = \frac{C_{123}}{z_{12}^{h_1+h_2-h_3} z_{23}^{h_2+h_3-h_1} z_{13}^{h_1+h_3-h_2}} \tag{3.14}$$

where C_{123} are the OPE coefficients that encode the fusion rules of the theory.

3.1.4 Scaling Behavior and Critical Exponents

Conformal field theory offers a natural language for describing scale-invariant systems, particularly near second-order phase transitions. In this framework, the conformal weights $(h, \bar{h})$ of a primary operator determine its scaling dimension and conformal spin:

$$\Delta = h + \bar{h}, \quad s = h - \bar{h} \tag{3.15}$$

The scaling dimension Δ governs the algebraic decay of correlation functions and corresponds to critical exponents characterizing the divergence of correlation lengths near criticality.

For example, the two-point function of a scalar primary operator exhibits power-law behavior:

$$\langle \phi(x)\phi(0)\rangle \sim \frac{1}{|x|^{2\Delta}} \tag{3.16}$$

which is a hallmark of critical systems and reflects long-range correlations in the absence of a characteristic scale.

doi:10.6342/NTU202501665

3.2 Boundary Conformal Field Theory

Boundary conformal field theory is a natural extension of two-dimensional conformal field theory to systems with boundaries. When a boundary is introduced, the full conformal symmetry is partially broken—only those transformations that preserve the boundary are retained.

This symmetry reduction leads to several key structural changes. First, it modified OPE involving interactions between bulk and boundary operators. Second, the boundary conditions on the stress-energy tensor, such as $T(z) = \bar{T}(\bar{z})$ on the boundary, ensuring the conservation of energy and momentum parallel to the boundary. Last, it altered correlation functions, which are constrained by the reduced conformal symmetry and depend on the geometry of the boundary.

Despite this symmetry reduction, conformal invariance continues to strongly constrain the theory—particularly the structure of correlation functions and the set of consistent boundary conditions. These constraints form the foundation for constructing boundary states, boundary operator expansions, and solving boundary CFT in both physical and mathematical contexts.

In BCFT, conformal invariance imposes continuity of the energy-momentum flow across the boundary. This requirement leads to a condition on the holomorphic and anti-holomorphic components of the stress-energy tensor:

$$T(z) = \bar{T}(\bar{z}) \quad \text{at } z = \bar{z} \tag{3.17}$$

This relation, known as the gluing condition, ensures the absence of momentum flux per-

doi:10.6342/NTU202501665

pendicular to the boundary and constrains the class of admissible boundary conditions.

In specific models, such as the free boson CFT, standard conformally invariant boundary conditions include:

- Dirichlet boundary conditions, which fix the field value at the boundary.
- Neumann boundary conditions, which fix the derivative (normal to the boundary) of the field.

More generally, each conformal boundary condition corresponds to a distinct boundary state in the closed-string channel, where spatial and temporal directions are interchanged. These boundary states are subject to nontrivial algebraic constraints, most notably, the Cardy condition, which ensures consistency of the theory under modular transformations. This requirement guarantees that the open-string (boundary Hilbert space) and closed-string (boundary state overlap) descriptions yield the same partition function. The Cardy condition places strong restrictions on the allowed boundary states and their relation to the bulk conformal data, ensuring modular invariance and overall physical consistency.

BCFT provides a powerful and versatile framework for analyzing critical systems defined on domains with boundaries, such as the upper half-plane or finite strips. It plays a central role across diverse areas of theoretical and applied physics. In condensed matter systems, BCFT offers a rigorous approach to understanding boundary critical phenomena and quantum impurity problems (e.g., the Kondo effect). In statistical mechanics, it governs the impact of boundary conditions in lattice models like the Ising models at criticality.

doi:10.6342/NTU202501665

In the context of this work, BCFT offers a robust theoretical framework for analyzing one-dimensional quantum systems with localized impurities or defects. By mapping these systems to boundary field theories, often using tools like the folding trick, one can reinterpret general non-Hermitian impurities within the language of conformal boundaries. This approach enables a precise treatment of scattering, reflection, and finite-size effects in terms of conformal data.

3.3 Boundary sine-Gordon model

In Refs. [7, 8], Polchinski and Maldacena et al. study the $c = 1$ BCFT with a sine-Gordon-type boundary interaction. The Lagrangian is given by:

$$L = \frac{1}{8\pi}\int_0^l d\sigma\,(\partial_\mu X)^2 - \frac{1}{2}\left(g_0 e^{iX(0)/\sqrt{2}} + \bar{g}_0 e^{-iX(0)/\sqrt{2}}\right), \tag{3.18}$$

where g_0 and $\bar{g}_0$ are boundary interaction couplings, satisfying the Hermitian condition

$$\bar{g}_0 = g_0^* \tag{3.19}$$

In these works, Maldacena et al. analyze the basic properties of the c=1 BCFT, describing a free boson with periodic boundary interaction and exhibiting an exactly solvable boundary S-matrix [7]. Polchinski et al. study a conformal field theory of a massless scalar with a periodic boundary interaction, solvable via fermionization. Their approach reveals the $SU(2)$ symmetry and a band-structured spectrum tunable by the boundary coupling

doi:10.6342/NTU202501665

[8].

In Ref. [9], the authors extend previous work to the general non-unitary case, presenting an exactly solvable boundary sine-Gordon model at the self-dual radius. This model can be mapped to free fermions and exhibits rich structures, such as $SL(2,\mathbb{C})$ boundary states, T-duality symmetry, and more general conformal boundary conditions.

The action in this formulation differs slightly from earlier works by the inclusion of a gauge term $A\partial_t X$, along with a reparameterization of the coupling constants g and $\bar{g}$:

$$g = -\frac{1}{\pi}\frac{g_0}{\sqrt{g_0\bar{g}_0}}\sin\pi\sqrt{g_0\bar{g}_0} \quad \bar{g} = -\frac{1}{\pi}\frac{\bar{g}_0}{\sqrt{g_0\bar{g}_0}}\sin\pi\sqrt{g_0\bar{g}_0} \tag{3.20}$$

When $g_0 = \bar{g}_0^*$, the condition $g = \bar{g}^*$ holds, and the unitarity bound $|g| \leq 1/\pi$ is always satisfied, ensuring that the theory remains unitary.

However, in the general non-Hermitian case where $g \neq \bar{g}$, the action takes the form

$$S = \frac{1}{4\pi}\int_{-\infty}^{\infty} dt \int_0^{\pi} ds \left(\partial_t X^2 - \partial_s X^2\right) - \int_{-\infty}^{\infty} dt \left(\frac{g}{2}e^{iX(t,0)} + \frac{\bar{g}}{2}e^{-iX(t,0)} + A\partial_t X(t,0)\right) \tag{3.21}$$

where $X(t,s)$ is a scalar field defined on a strip $(t,s) \in R \otimes [0,\pi]$, and $g, \bar{g} \in \mathbb{C}$ are independent coupling constants.

In the bulk, the theory is free and governed by the standard wave equation:

$$(\partial_t^2 - \partial_s^2)X(t,s) = 0. \tag{3.22}$$

The interaction is localized at the boundary $s = 0$, where the field satisfies the nonlinear

doi:10.6342/NTU202501665

boundary condition:

$$-\partial_s X(t,0) + i\frac{g}{2}e^{iX(t,0)} - i\frac{\bar{g}}{2}e^{-iX(t,0)} = 0. \tag{3.23}$$

At the opposite boundary, $s = \pi$, we consider several types of boundary conditions: the Dirichlet condition, $\partial_t X(t,\pi) = 0$, the Neumann condition, $\partial_s X(t,\pi) = 0$, as well as generalized conditions involving a periodic boundary operator, which may include additional interaction parameters. The couplings g and $\bar{g}$ are treated as independent complex variables, not constrained to be complex conjugates. Crucially, the boundary interaction is known to be exactly marginal, ensuring that the perturbed theory retains conformal invariance for arbitrary values of g and $\bar{g}$.

3.3.1 Fermionization

To facilitate the construction of the boundary state $|B\rangle$ in fermionic variables, we begin by doubling the bosonic degrees of freedom. This is achieved by introducing an auxiliary scalar field Y, which satisfies Dirichlet boundary conditions at all spatial boundaries. The system is then described by the Euclidean action:

$$S = \frac{1}{4\pi}\int_{-\infty}^{\infty} d\tau \int_0^{2\pi} d\sigma \left(\partial_\tau X^2 + \partial_\sigma X^2 + \partial_\tau Y^2 + \partial_\sigma Y^2\right) \tag{3.24}$$

where both $X(\tau,\sigma)$ and $Y(\tau,\sigma)$ are compactified bosonic fields defined on a cylinder, with spatial coordinate $\sigma \in [0, 2\pi]$ and Euclidean time $\tau \in \mathbb{R}$. The inclusion of the field Y enables fermionization, allowing the combination $X \pm Y$ to be mapped to chiral components of a Dirac fermion. The boundary state $|B, D\rangle$, which incorporates the nonlinear boundary interaction in the X-sector and imposes Dirichlet conditions on the Y-field, must

doi:10.6342/NTU202501665

satisfy the following operator constraints:

$$\left[-\frac{1}{2\pi}\partial_\tau X(0,\sigma) + i\frac{g}{2}e^{iX(0,\sigma)} - i\frac{\bar{g}}{2}e^{-iX(0,\sigma)}\right]|B,D\rangle = 0 \tag{3.25}$$

$$Y(0,\sigma)|B,D\rangle = 0 \tag{3.26}$$

This formulation sets the stage for fermionization, as the linear combinations $X \pm Y$ correspond to chiral bosons that map naturally to left- and right-moving components of a Dirac fermion. The theory for Y is free, decoupled, and exactly solvable. Its contribution to quantities such as the partition function can be explicitly isolated and factored out, allowing one to focus solely on the dynamics of the X-sector. The primary role of Y is to facilitate the mapping to fermionic variables, as described below. We define new bosonic fields:

$$\phi_1 = \frac{1}{\sqrt{2}}(X+Y), \quad \phi_2 = \frac{1}{\sqrt{2}}(X-Y) \tag{3.27}$$

which enable standard bosonization into a system of two species of free Dirac fermions. The corresponding fermion bilinear relates to bosonic currents as:

$$:\psi_{1L}^\dagger(z)\psi_{1L}(z): = i\sqrt{2}\,\partial_\tau\phi_{1L}(z), \qquad :\psi_{2L}^\dagger(z)\psi_{2L}(z): = -i\sqrt{2}\,\partial_\tau\phi_{2L}(z)$$

$$:\psi_{1R}^\dagger(\bar{z})\psi_{1R}(\bar{z}): = -i\sqrt{2}\,\partial_\tau\phi_{1R}(\bar{z}), \qquad :\psi_{2R}^\dagger(\bar{z})\psi_{2R}(\bar{z}): = i\sqrt{2}\,\partial_\tau\phi_{2R}(\bar{z})$$

where $z = \tau + i\sigma, \bar{z} = \tau - i\sigma$. In terms of these fermionic variables, the action takes the form:

$$S = \frac{i}{2\pi}\int_{-\infty}^{\infty} d\tau \int_0^{2\pi} d\sigma \left(\psi_{aL}^\dagger(\partial_\tau + i\partial_\sigma)\psi_{aL} + \psi_{aR}^\dagger(\partial_\tau - i\partial_\sigma)\psi_{aR}\right) \tag{3.28}$$

The fermionic formulation exhibits an explicit $SU(2)_L \times SU(2)_R$ chiral symmetry. Owing to the holomorphic structure of the chiral currents, this symmetry extends to two inde-

doi:10.6342/NTU202501665

pendent level-1 $SU(2)$ Kac-Moody algebras. The left-moving affine $SU(2)$ currents are generated by:

$$J_L^a(z) = \frac{1}{2} : \psi_L^\dagger(z)\, \sigma^a\, \psi_L(z) : \qquad \sigma^a = \text{Pauli matrices} \tag{3.29}$$

Explicitly, these currents can be expressed as:

$$J_L^+(z) = \psi_{L1}^\dagger(z)\psi_{L2}^\dagger(z), \quad J_L^-(z) = \psi_{L2}(z)\psi_{L1}(z), \quad J_L^3(z) = \frac{1}{2} : \psi_L^\dagger(z)\psi_L(z) : \tag{3.30}$$

The boundary condition at $\sigma = 0$, originally nonlinear in the bosonic language, now becomes linear in terms of fermionic bilinear. It imposes the following constraint on the boundary state condition:

$$\Big[: \psi_L^\dagger \sigma^3 \psi_L : - : \psi_R^\dagger \sigma^3 \psi_R : + \pi g\, \psi_L^\dagger (1+\sigma^3)\psi_R - \pi \bar{g}\, \psi_L^\dagger (1-\sigma^3)\psi_R \Big] \, |B, D\rangle = 0 \tag{3.31}$$

This linear structure makes the problem of constructing the boundary state more tractable in the fermionic representation. It is known that certain boundary states are related by global $SU(2)$ rotations acting on the left-moving fermionic fields. For instance, the Dirichlet–Dirichlet ($|DD\rangle$) and Neumann–Dirichlet ($|ND\rangle$) boundary conditions are given by:

$$(\psi_R(0,\sigma) - \psi_L(0,\sigma))\, |DD\rangle = 0, \qquad \Big(\psi_R^\dagger(0,\sigma) + \psi_L^\dagger(0,\sigma)\Big)\, |DD\rangle = 0 \tag{3.32}$$

$$\big(\psi_R(0,\sigma) + i\sigma^1 \psi_L(0,\sigma)\big)\, |ND\rangle = 0, \qquad \Big(\psi_R^\dagger(0,\sigma) + \psi_L^\dagger(0,\sigma) i\sigma^1\Big)\, |ND\rangle = 0 \tag{3.33}$$

doi:10.6342/NTU202501665

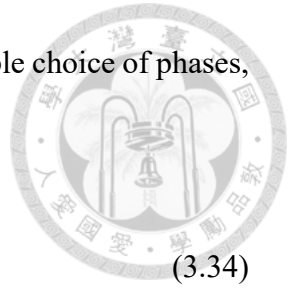

These conditions are related by a global $SU(2)$ rotation. With a suitable choice of phases, the corresponding boundary states are also related via:

$$|DD\rangle = e^{-i\pi J_L^1}|ND\rangle \tag{3.34}$$

where J_L^a are the generators of the left-moving $SU(2)$ Kac-Moody algebra. As argued in [7], the interacting boundary state $|BD\rangle$ can also be obtained from the $|ND\rangle$ state by a global rotation. To explore this idea, we introduce the ansatz:

$$|BD\rangle = e^{-i\theta\, J_L}|ND\rangle \tag{3.35}$$

where $\theta \in \mathbb{C}$ in the most general case, so the transformation lies in $SL(2,\mathbb{C})$. Since the generators J_L^a act only on the X-boson sector, the Dirichlet condition on the Y-boson remains unaffected. Under this transformation, the fermionic fields transform as:

$$e^{-i\theta\cdot J_L}\,\psi_L\, e^{i\theta\cdot J_L} = U\psi_L, \quad e^{-i\theta\cdot J_L}\,\psi_L^\dagger\, e^{i\theta\cdot J_L} = \psi_L^\dagger U^{-1}, \quad U = e^{i\theta\cdot\sigma/2} \tag{3.36}$$

The unit determinant condition ensures that only the X-sector is affected. This transformation implies that the boundary state $|BD\rangle$ satisfies the gluing condition:

$$\left(\psi_R(0,\sigma) + i\sigma^1 U\psi_L(0,\sigma)\right)|BD\rangle = 0, \quad \left(\psi_R^\dagger(0,\sigma) + \psi_L^\dagger(0,\sigma)U^{-1}i\sigma^1\right)|BD\rangle = 0 \tag{3.37}$$

This class of boundary states automatically satisfies conformal invariance, as the energy-momentum tensor is $SU(2)_L{\times}SU(2)_R$-invariant and quadratic in the fermion fields:

$$(L_n - \tilde{L}_{-n})|BD\rangle = 0 \tag{3.38}$$

doi:10.6342/NTU202501665

A specific solution to the boundary condition is obtained when the matrix U takes the form:

$$U = \begin{bmatrix} e^{-2\pi iA}\sqrt{1-\pi^2 g\bar{g}} & -i\pi g \\ -i\pi\bar{g} & e^{2\pi iA}\sqrt{1-\pi^2 g\bar{g}} \end{bmatrix} \tag{3.39}$$

3.3.2 Partition Function

Following [9], the partition function of a theory with distinct boundary conditions at each end of the strip can be written as:

$$Z_{B_1B_2}[\beta] = e^{\beta/24}\sum_{n\in\mathbb{Z}} e^{-\beta(n+\delta)^2}\prod_{k=1}^{\infty}\frac{1}{1-e^{-\beta k}}, \tag{3.40}$$

where the factor $\delta[A, g, \bar{g}]$ encodes the effect of boundary interactions and phase shifts due to boundary couplings. If the boson is compactified at the self-dual radius, the zero-mode spectrum becomes discrete, and the parameter A remains fixed—treated as a modulus rather than a dynamical variable. In this case, for boundary sine-Gordon interactions with complex couplings $g_1, \bar{g}_1$ and $g_2, \bar{g}_2$, the boundary-induced momentum shift takes the form:

$$\delta[A, g, \bar{g}] = \frac{1}{2\pi}\cos^{-1}\left[cos(2\pi A)\sqrt{1-\pi^2 g_1\bar{g}_1}\sqrt{1-\pi^2 g_2\bar{g}_2} + \frac{\pi^2}{2}(g_1\bar{g}_2 + \bar{g}_1 g_2)\right] \tag{3.41}$$

This expression captures how the interference between boundary couplings and the zero-mode phase A controls the spectral flow across boundary conditions, and directly contributes to finite-size energy shifts.

In our setup, we impose a general boundary condition B, characterized by the complex couplings $g, \bar{g}$, at the boundary $s = 0$, and a Dirichlet boundary condition at $s = \pi$.

doi:10.6342/NTU202501665

The corresponding finite-temperature partition function takes the form:

$$Z_{BD}[\beta] = e^{\beta/24} \sum_{n\in\mathbb{Z}} e^{-\beta(n+\delta)^2} \prod_{k=1}^{\infty} \frac{1}{1-e^{-\beta k}} \tag{3.42}$$

where the parameter δ encodes the effect of the boundary interaction and is given by:

$$\delta = \frac{1}{2\pi} \cos^{-1}\left(\frac{\pi}{2}(g+\bar{g})\right). \tag{3.43}$$

This parameter represents a boundary-induced momentum shift and determines the structure of the conformal spectrum. In particular, the ground state energy of the system is:

$$E_0 = \delta^2 - \frac{1}{24} \tag{3.44}$$

while the energies of excited states are given by:

$$E = (n+\delta)^2 + N - \frac{1}{24} \tag{3.45}$$

with $n \in \mathbb{Z}$ representing the quantized momentum sector and $N \in \mathbb{N}_0$ labeling oscillator excitations.

This structure reflects the standard BCFT decomposition into Virasoro characters, with δ effectively controlling the conformal weight of the primary associated with the boundary condition. The condition $|\frac{\pi}{2}(g+\bar{g})| \leq 1$ ensures that δ remains real spectrum.

doi:10.6342/NTU202501665

doi:10.6342/NTU202501665

Chapter 4 Non-Hermitian Critical Systems with Impurities and BCFT

Building on the work of Takasan et al. [1][2], who analyzed the L^{-1} correction to the ground state energy, we extend their framework to the non-Hermitian case. In the Hermitian setting, the transmission coefficient T_F determines whether the barrier acts as a relevant or irrelevant perturbation under renormalization group (RG) flow, flowing to either a perfectly reflecting or transmitting fixed point, corresponding to Neumann or Dirichlet boundary conditions, respectively. For free fermions (K = 1), the barrier is exactly marginal, leading to a continuous family of boundary conditions described by an $\mathrm{SU}(2)$ S-matrix, parametrized by an effective barrier strength g as introduced in [8], with $T_F = \cos(\pi g)$ and phase shift $\Delta = \pi|g| = \arccos(T_F)$. In our work, we generalize this analysis to systems with non-Hermitian couplings. Using the folding trick, we identify the relationship between the coupling constant v in the lattice model and the effective parameter g, and explore how this affects the emergent boundary conditions in the BCFT picture. We also compute the ground state energy at $k = \pi/2$, the Fermi level, where bosonization is particularly effective, and show that the resulting critical energy matches the predictions of BCFT.

doi:10.6342/NTU202501665

4.1 Single Defect Models

We consider a tight-binding model with an impurity between site $i = 0, 1$, as shown in Fig. 4.1, described by the following Hamiltonian:

$$H = t_0 \sum_{i \neq 0} (c_i^\dagger c_{i+1} + h.c.) + v c_0^\dagger c_1 + \bar{v} c_1^\dagger c_0 \tag{4.1}$$

here, t_0 is the uniform nearest-neighbor hopping amplitude, and the impurity is encoded in two terms: a modified hopping amplitude v ($\bar{v}$) across the bond between sites 0 and 1, representing a single-bond disorder. The creation (annihilation) operators $c_i^\dagger$ (c_i) satisfy standard fermionic anti-commutation relations.

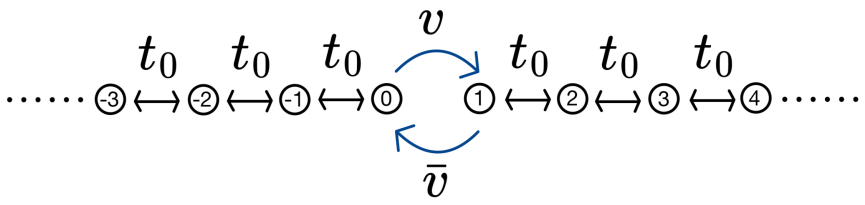

Figure 4.1: A tight-binding model with uniform hopping t_0 and impurity between site $i = 0, 1$

Noticing that $v \in \mathbb{C}$ is, in general, a complex-valued hopping amplitude across the impurity bond between sites 0 and 1. The Hamiltonian remains Hermitian if and only if $v = \bar{v}^\dagger$. For $v \neq \bar{v}^\dagger$, the system becomes non-Hermitian, allowing for asymmetric transport, complex eigenvalues, and other non-Hermitian phenomena relevant to open quantum systems and effective models with gain or loss.

doi:10.6342/NTU202501665

4.2 Scattering Matrix (S-matrix) Formalism

To analyze the scattering properties of the impurity, we begin by assuming well-defined asymptotic behavior for the wavefunction $\psi_k(x)$ away from the defect. The general scattering ansatz takes the form:

$$\psi_k(x) \equiv \tilde{\psi}_k^+ e^{ikx} + \tilde{\psi}_k^- e^{-ikx}, \quad x \leq 0 \tag{4.2}$$

$$\psi_k(x) \equiv \psi_k^+ e^{ikx} + \psi_k^- e^{-ikx}, \quad x > 0 \tag{4.3}$$

where k is the momentum of the incoming particle. The coefficients $\tilde{\psi}_k^+$ and ψ_k^+ correspond to right-moving (forward) components, while $\tilde{\psi}_k^-$ and ψ_k^- describe left-moving (reflected or incoming from the right) components. This form captures the scattering due to the impurity localized at the bond between $x = 0$ and $x = 1$.

Using the asymptotic wavefunction components, we define the scattering matrix S_k as:

$$S_k \equiv \begin{pmatrix} T_k^+ & R_k^- \\ R_k^+ & T_k^- \end{pmatrix} \tag{4.4}$$

where $T_k^\pm$ denote the transmission amplitudes for particles incident from the left $(+)$ and right $(-)$, while $R_k^\pm$ denote the corresponding reflection amplitudes. The scattering relation connects incoming and outgoing wave amplitudes via a momentum-dependent scattering matrix S_k. Explicitly, the relation reads:

$$\begin{pmatrix} \psi_k^+ \\ \tilde{\psi}_k^- \end{pmatrix} = S_k \begin{pmatrix} \tilde{\psi}_k^+ \\ \psi_k^- \end{pmatrix} \tag{4.5}$$

doi:10.6342/NTU202501665

here, $\tilde{\psi}_k^+$ and ψ_k^- are the incoming amplitudes from the left and right, respectively, while ψ_k^+ and $\tilde{\psi}_k^-$ are the corresponding outgoing amplitudes. To streamline notation, we define the composite vectors for incoming and outgoing states as:

$$\psi_{\text{in}} = \begin{pmatrix} \tilde{\psi}^+ \\ \psi^- \end{pmatrix}, \quad \psi_{\text{out}} = \begin{pmatrix} \tilde{\psi}^- \\ \psi^+ \end{pmatrix} \tag{4.6}$$

so that the scattering relation takes the compact form:

$$\psi_{\text{out}} = S_k(v, \bar{v}, t_0)\, \psi_{\text{in}}. \tag{4.7}$$

where S_k may depend not only on the momentum k but also on the complex boundary couplings v, $\bar{v}$, and the uniform hopping amplitude parameter t_0.

4.2.1 Connection to Transport Properties

The scattering matrix S_k plays a central role in characterizing quantum transport across the impurity. Of particular interest are the transmission amplitudes $T_k^{\pm}$, which quantify the probability amplitudes for a particle to transmit through the defect from left to right (T_k^+) and from right to left (T_k^-). The corresponding transmission probabilities, $|T_k^{\pm}|^2$, provide direct access to measurable transport observables, such as the conductance and shot noise. These quantities encode the nontrivial influence of the boundary interaction on dynamical response properties of the system. In Hermitian systems, unitarity of the scattering matrix S_k guarantees conservation of probability. This implies that the total outgoing probability equals the incoming one, yielding the relations:

$$|T_k^+|^2 + |R_k^+|^2 = 1, \qquad |T_k^-|^2 + |R_k^-|^2 = 1 \tag{4.8}$$

doi:10.6342/NTU202501665

In contrast, for non-Hermitian systems, such as those involving complex boundary couplings $v \neq \bar{v}^*$, the S-matrix is generally non-unitary. This leads to possible amplification or attenuation of wave amplitudes, reflecting non-conservative transport. Physically, such deviations from unitarity are interpreted as gain/loss mechanisms or leakage into auxiliary degrees of freedom, and are characteristic of open or dissipative quantum systems. Within the framework of BCFT, the coefficients appearing in the finite-size energy spectrum, such as those proportional to L^{-1}, can be interpreted as elements of a boundary scattering matrix (S-matrix). This matrix characterizes how conformal excitations interact with the boundary, determining whether they are reflected, transmitted, or subject to phase shifts. This correspondence establishes a profound connection between microscopic transport properties and universal features of critical phenomena described by BCFT.

4.2.2 S-matrix with Hermiticity

In Refs. [1, 2], Takasan *et al.* computed the scattering matrix for Hermitian impurity configurations. In particular, for the case of single-bond disorder, where the modified hopping amplitude v satisfies the Hermiticity condition $v = \bar{v}^\dagger$, the transmission and reflection amplitudes can be explicitly obtained as:

$$\begin{aligned} T_k^{\pm} &= \frac{2t_0 v \sin k}{(t_0^2 + v^2)\sin k + i(t_0^2 - v^2)\cos k} \\ R_k^{\pm} &= -e^{\pm ik}\frac{i(t_0^2 - v^2)}{(t_0^2 + v^2)\sin k + i(t_0^2 - v^2)\cos k} \end{aligned} \tag{4.9}$$

This simple yet analytically tractable model captures the key features of coherent quantum scattering at a boundary or localized impurity. The unitarity conditions (4.8):

$$|T_k^{\pm}|^2 + |R_k^{\pm}|^2 = 1$$

doi:10.6342/NTU202501665

can be verified directly from the expressions above, confirming that probability flux is conserved. The parameter v effectively tunes the boundary condition, enabling interpolation between limiting cases of perfect reflection and perfect transmission. In the language of boundary conformal field theory, this corresponds to a continuous deformation between Neumann and Dirichlet boundary conditions. This unitarity plays a key role in interpreting the impurity's effect within both lattice models and their low-energy continuum (BCFT) descriptions.

4.2.3 Generalize to non-Hermitian case

The momentum-dependent scattering matrix S_k for a impurity with complex boundary coupling v, $\bar{v}$ is given by:

$$S_k = \begin{pmatrix} \dfrac{(1-e^{2ik})vt_0}{t_0^2 - v\bar{v}\,e^{2ik}} & -\dfrac{t_0^2 - v\bar{v}}{t_0^2 - v\bar{v}\,e^{2ik}} \\ -\dfrac{t_0^2 - v\bar{v}}{t_0^2 - v\bar{v}\,e^{2ik}}e^{2ik} & \dfrac{(1-e^{2ik})\bar{v}t_0}{t_0^2 - v\bar{v}\,e^{2ik}} \end{pmatrix} \tag{4.10}$$

where t_0 is the bulk hopping amplitude and k is the momentum of the incoming wave. This matrix encodes the complete set of reflection and transmission amplitudes for plane-wave scattering at the boundary. When $v = \bar{v}^\dagger$, the system is Hermitian, and S_k is manifestly unitary, preserving the total probability current. However, when $v \neq \bar{v}^\dagger$, the boundary becomes non-Hermitian, leading to a generally non-unitary S_k. This results in asymmetric reflection probabilities and the potential for gain or loss in wave amplitude. Such behavior is indicative of non-conservative transport and is closely tied to emergent features of non-unitary boundary conformal field theory (BCFT).

doi:10.6342/NTU202501665

4.2.4 Critical Point Behavior

A particularly significant momentum in one-dimensional lattice systems is $k = \pm\pi/2$, corresponding to half-filling in the tight-binding chain. At this momentum, the Fermi level is pinned at the band center of the non-interacting system, marking the critical point of the metallic phase. This point plays a central role in low-energy continuum descriptions and is pivotal in conformal field theory (CFT) analyses. At $k = \pm\pi/2$, the lattice phase factor simplifies to $e^{2ik} = -1$, leading to a simplified form of the scattering matrix S_k from Eq. (4.10). Specifically, we obtain:

$$\mathcal{S}_{k=\frac{\pi}{2}} = \begin{pmatrix} \dfrac{2vt_0}{t_0^2 + v\bar{v}} & -\dfrac{t_0^2 - v\bar{v}}{t_0^2 + v\bar{v}} \\ \dfrac{t_0^2 - v\bar{v}}{t_0^2 + v\bar{v}} & \dfrac{2\bar{v}t_0}{t_0^2 + v\bar{v}} \end{pmatrix} \tag{4.11}$$

In the Hermitian limit, where $v = \bar{v}^\dagger$, the S-matrix becomes manifestly unitary. The transmission amplitude is then:

$$T^+ = (T^-)^* = \frac{2vt_0}{t_0^2 + |v|^2} \tag{4.12}$$

and the reflection amplitude is:

$$R^+ = -R^- = \frac{t_0^2 - |v|^2}{t_0^2 + |v|^2} \tag{4.13}$$

both of which satisfy the conservation law from Eq. (4.8):

$$|T_k^\pm|^2 + |R_k^\pm|^2 = 1$$

This confirms probability conservation and illustrates a continuous crossover from

doi:10.6342/NTU202501665

full reflection ($v \to 0$) to perfect transmission ($v = \bar{v} = t$).

For general complex values $v \neq \bar{v}^\dagger$, the scattering matrix becomes non-unitary. The off-diagonal elements develop complex, asymmetric contributions, leading to reflection asymmetry and the emergence of gain or loss. The total outgoing probability, defined as the sum of squared transmission and reflection amplitudes, becomes:

$$|R^+(k)|^2 + |T^+(k)|^2 = \frac{\left|1 - e^{2ik}\right|^2 |v|^2 t_0^2 + \left|e^{2ik}\right|^2 |t_0^2 - v\bar{v}|^2}{\left|t_0^2 - v\bar{v}e^{2ik}\right|^2} \tag{4.14}$$

at $k = \pm\pi/2$, where $e^{2ik} = -1$, this simplifies to:

$$|T^+|^2 + |R^+|^2\Big|_{k=\frac{\pi}{2}} = \frac{4|v|^2 t_0^2 + |t_0^2 - v\bar{v}|^2}{|t_0^2 + v\bar{v}|^2} \tag{4.15}$$

This expression makes it explicit that unitarity is generically violated for complex $v, \bar{v}$, with the deviation from unity governed by the imaginary part of $v\bar{v}$. Such behavior signals the presence of amplification (gain) or attenuation (loss), indicating that the impurity functions as a source or sink of probability current, a defining feature of non-Hermitian boundary physics.

Such non-unitarity reflects norm non-conservation in the scattering states and indicates that the impurity can act as a source or sink of probability current. The poles of the scattering matrix in the complex v-plane encode resonant features and may be interpreted in terms of decay rates or emergent non-Hermitian criticality.

At $k = \pm\pi/2$, the lattice system lies at a critical point described by a massless Dirac theory in the continuum limit. The simplified matrix $S_{k=\pi/2}$ directly encodes the boundary condition for chiral fermions. Within the boundary conformal field theory (BCFT) frame-

doi:10.6342/NTU202501665

work, the dependence on $v, \bar{v}$ instead of $|v|^2$ signals unitarity breaking, though the analytic structure remains intact. This suggests possible consistency with non-unitary CFT.

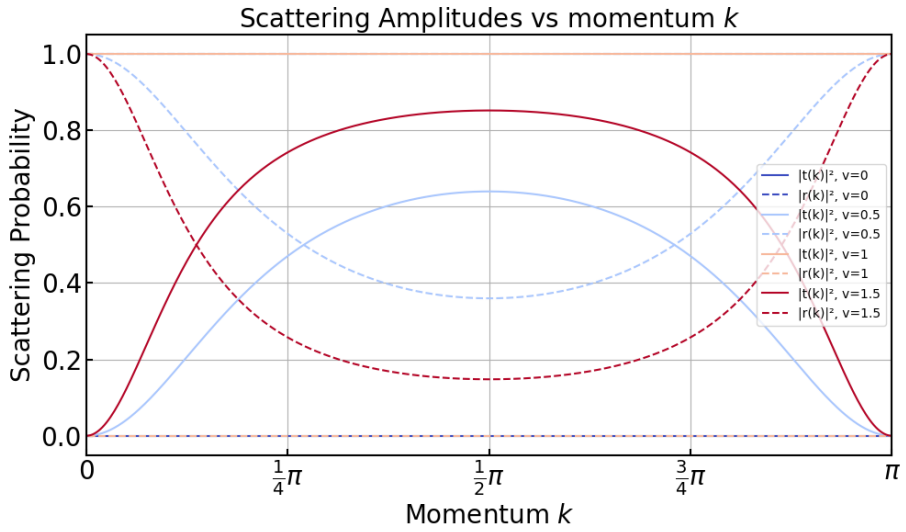

Figure 4.2: Scattering Amplitudes vs momentum k. Both reflection and transmission amplitudes reach extrema at $k = \pi/2$.

The relation $T^{+} = T^{-\dagger}$ holds only in the Hermitian case. More generally, $S^{-1} \neq S^{\dagger}$, reflecting broken left-right symmetry. This asymmetry is a hallmark of non-reciprocal or direction-dependent transport. As such, $k = \pm\pi/2$ serves as a diagnostic momentum: it yields compact analytic expressions while remaining acutely sensitive to complex coupling asymmetries.

Their dynamics dominate low-energy transport near half-filling and naturally lead to the emergence of left- and right-moving modes in a linearized continuum description. In field-theoretic terms, this corresponds to expanding around the Fermi points, yielding a massless Dirac theory that captures the critical behavior.

In summary, analyzing boundary scattering at $k = \pm\pi/2$ offers a clear diagnostic of impurity effects at criticality. It connects microscopic lattice details with macroscopic transport properties, providing a bridge between tight-binding models and boundary conformal field theories.

doi:10.6342/NTU202501665

4.3 Correspondence with BCFT

We now explore the connection between BCFT and non-Hermitian systems. It is natural to relate (1+1)-dimensional fermionic CFT to lattice models, where boundary terms in BCFT correspond to impurities in the lattice system. For example, Refs. [37, 38] investigate the application of conformal field theory to the Kondo effect. In our work, we establish a connection between BCFT with specific boundary terms and non-Hermitian impurities by employing the folding trick. Through this approach, we identify a correspondence between the boundary state in BCFT and the scattering matrix of the non-Hermitian system.

4.3.1 Parameterization

Recall the general form of the non-Hermitian scattering matrix, given by Eq. (4.10):

$$S_k = \begin{pmatrix} \dfrac{(1-e^{2ik})\, v\, t_0}{t_0^2 - v\bar{v}\, e^{2ik}} & -\dfrac{t_0^2 - v\bar{v}}{t_0^2 - v\bar{v}\, e^{2ik}} \\ -\dfrac{t_0^2 - v\bar{v}}{t_0^2 - v\bar{v}\, e^{2ik}} e^{2ik} & \dfrac{(1-e^{2ik})\, \bar{v}\, t_0}{t_0^2 - v\bar{v}\, e^{2ik}} \end{pmatrix}$$

At the special momenta $k = \pm\pi/2$, the exponential factor simplifies due to $e^{2ik} = e^{\pm i\pi} = -1$. Substituting this into the general form yields:

$$S_{k=\frac{\pi}{2}} = \begin{pmatrix} \dfrac{2vt_0}{t_0^2 + v\bar{v}} & -\dfrac{t_0^2 - v\bar{v}}{t_0^2 + v\bar{v}} \\ \dfrac{t_0^2 - v\bar{v}}{t_0^2 + v\bar{v}} & \dfrac{2\bar{v}t_0}{t_0^2 + v\bar{v}} \end{pmatrix} \tag{4.16}$$

Here, the reflection amplitude picks up a sign depending on the direction of incidence:

$$R^+ = -R^-, \quad \text{since} \quad e^{2ik} = -1$$

doi:10.6342/NTU202501665

This sign flip reflects the asymmetry of reflection in the non-Hermitian setting and is a direct manifestation of the non-reciprocal scattering behavior of the system. It also suggests that time-reversal symmetry is broken unless $v = \bar{v}^\dagger$, where the system becomes Hermitian and the scattering matrix is symmetric.

Furthermore, this structure should be compared to the boundary U-matrix from Eq. (3.39):

$$U = \begin{bmatrix} e^{-2\pi i A}\sqrt{1-\pi^2 g\bar{g}} & -i\pi g \\ -i\pi\bar{g} & e^{2\pi i A}\sqrt{1-\pi^2 g\bar{g}} \end{bmatrix}$$

which defines the gluing condition for left- and right-moving fermions in the boundary state formalism. Comparing $S_{k=\pi/2}$ and U, one observes structural similarities in how the coupling v (or g) enters the expressions, further reinforcing the identification of scattering data with conformal boundary conditions.

We now make a key identification between the scattering matrix $S_{k=\pi/2}$ and the conformal boundary gluing condition encoded by the matrix U. Recall the fermionic boundary condition defining the boundary state $|BD\rangle$, given by Eq (3.37):

$$\left(\psi_R(0,\sigma) + i\sigma^1 U\psi_L(0,\sigma)\right)|BD\rangle = 0, \quad \left(\psi_R^\dagger(0,\sigma) + \psi_L^\dagger(0,\sigma)U^{-1}i\sigma^1\right)|BD\rangle = 0$$

This condition defines how left- and right-moving fermions are matched at the boundary, with $U \in SL(2,\mathbb{C})$ encoding the boundary interaction structure. Comparing with the explicit form of the scattering matrix at $k = \pi/2$:

$$\mathcal{S}_{k=\frac{\pi}{2}} = \begin{pmatrix} \dfrac{2vt_0}{t_0^2+v\bar{v}} & -\dfrac{t_0^2-v\bar{v}}{t_0^2+v\bar{v}} \\ \dfrac{t_0^2-v\bar{v}}{t_0^2+v\bar{v}} & \dfrac{2\bar{v}t_0}{t_0^2+v\bar{v}} \end{pmatrix} = \begin{bmatrix} \pi\bar{g} & ie^{2\pi i A}\sqrt{1-\pi^2 g\bar{g}} \\ ie^{-2\pi i A}\sqrt{1-\pi^2 g\bar{g}} & \pi g \end{bmatrix} = i\sigma^1 U$$

The relations for g and $\bar{g}$ derived above encode how the complex lattice boundary cou-

doi:10.6342/NTU202501665

plings $v, \bar{v}$ map onto the continuum boundary sine-Gordon couplings. This mapping is especially meaningful at the critical momentum $k = \pi/2$, where the system reaches the critical point and the CFT description becomes most accurate. At this point, the scattering matrix takes on a particularly simple and symmetric form, allowing it to be written as:

$$\mathcal{S}_{k=\pi/2} = i\sigma^1 U \tag{4.17}$$

where U is the gluing matrix characterizing the boundary condition in the fermionic formulation of BCFT. By matching the elements of the scattering matrix to $i\sigma^1 U$, one obtains the explicit parametrization:

$$\bar{g} = \frac{1}{\pi} \cdot \frac{2vt_0}{t_0^2 + v\bar{v}}, \quad g = \frac{1}{\pi} \cdot \frac{2\bar{v}t_0}{t_0^2 + v\bar{v}}, \quad A = \frac{1}{4} \tag{4.18}$$

The identification $A = 1/4$ follows naturally from comparing the periodicity conditions in momentum and real space. For a finite system of length L, the periodicity of the scattering wavefunctions is given by:

$$\tilde{\psi}_k^+ = \psi_k^+ e^{ikL}, \qquad \tilde{\psi}_k^- = \psi_k^- e^{-ikL} \tag{4.19}$$

while the boundary phase twist in the CFT appears as:

$$\Psi_E(x + 2\pi) = e^{-2\pi i A} \Psi_E(x) \tag{4.20}$$

Equating the two expressions at $k = \pi/2$ yields $A = k/(2\pi) = 1/4$, confirming the physical consistency of the parametrization in Eq. (4.18).

Moreover, we can invert this mapping to express the lattice boundary coupling $v(\bar{v})$

doi:10.6342/NTU202501665

in terms of the continuum parameters g and $\bar{g}$. The result is:

$$\frac{v}{t_0} = \begin{cases} \dfrac{1 \pm \sqrt{1 - \pi^2 g\bar{g}}}{\pi g}, & \bar{v} \neq 0 \\ \dfrac{\pi \bar{g}}{2}, & \bar{v} = 0 \\ \dfrac{2}{\pi g}, & \bar{v} \to \infty \end{cases} \tag{4.21}$$

This expression provides a parametric map from the bulk coupling space $(v, \bar{v}, t_0)$ to the effective boundary interaction space $(g, \bar{g})$, describing how the microscopic impurity couplings control the boundary behavior in the low-energy effective theory. Notably, the critical value $g\bar{g} = \frac{1}{\pi^2}$ marks the conformal boundary coupling limit, beyond which the square root becomes imaginary and the theory depart from unitarity.

4.3.2 Folding Trick

The correspondence between the bulk impurity model, as encoded in the scattering matrix S_k, and the boundary state formulation of BCFT is made even more transparent via the folding trick. Illustrated in Fig. 4.3, the folding trick reformulates a point-like impurity in a 1D system into a boundary condition in a doubled (folded) theory.

In this picture, incoming and outgoing wave modes are redefined as two-component spinors:

$$\psi_{\text{in}} = \begin{pmatrix} \tilde{\psi}^+ \\ \psi^- \end{pmatrix}, \qquad \psi_{\text{out}} = \begin{pmatrix} \tilde{\psi}^- \\ \psi^+ \end{pmatrix} \tag{4.22}$$

where $\tilde{\psi}\pm$ originate from the negative x-axis (folded branch), and $\psi\pm$ correspond to the positive x-axis (unfolded branch). The impurity at the origin becomes a boundary in the

doi:10.6342/NTU202501665

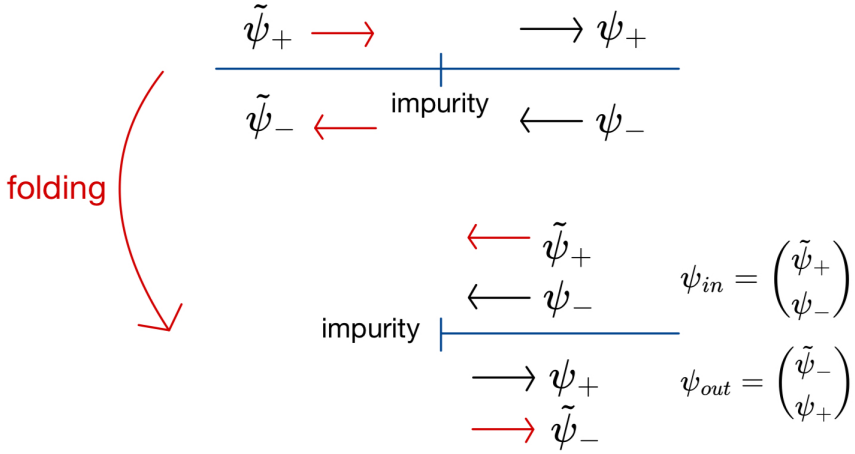

Figure 4.3: Folding trick in lattice systems: a single impurity becomes a boundary problem in a doubled (folded) theory

folded theory, and its scattering properties are encoded in a boundary condition:

$$\psi_{\text{out}} = S_k(v, \bar{v}, t_0)\psi_{\text{in}} \tag{4.23}$$

This relation formally matches the gluing condition used in constructing boundary states. By applying the folding trick, the impurity located at the origin of a one-dimensional wire can be reformulated as a boundary problem. Thus, the folding trick not only offers a conceptual bridge between impurity models and boundary field theory but also serves as a computational tool for translating scattering data into conformal boundary data.

To gain a clearer physical interpretation of the parameter space, we now consider the boundary conditions arising from the conformal field theory action Eq. (3.21):

$$S = \frac{1}{4\pi}\int_{-\infty}^{\infty} dt \int_0^{\pi} ds \left(\partial_t X^2 - \partial_s X^2\right) - \int_{-\infty}^{\infty} dt \left(\frac{g}{2} e^{iX(t,0)} + \frac{\bar{g}}{2} e^{-iX(t,0)} + A\partial_t X(t,0)\right)$$

where the interaction is localized at the boundary $s = 0$, and the parameters $g, \bar{g} \in \mathbb{C}$ control the strength and phase of the boundary sine-Gordon interaction. The resulting

doi:10.6342/NTU202501665

boundary equation of motion is:

$$-\partial_s X(t,0) + i\frac{g}{2}e^{iX(t,0)} - i\frac{\bar{g}}{2}e^{-iX(t,0)} = 0 \tag{4.24}$$

This expression makes it evident that the type of boundary condition is governed by the values of g and $\bar{g}$. When the boundary interaction vanishes ($g = \bar{g} = 0$), the equation reduces to:

$$\partial_s X(t,0) = 0 \tag{4.25}$$

which corresponds to a free boundary, or Neumann condition. In this regime, fluctuations of the field are unconstrained at the boundary.

In contrast, when $|g| \to \frac{1}{\pi}$, where the critical coupling strength is, the interaction becomes maximally strong, and the field is effectively pinned at a fixed value. In this limit, the dynamics impose:

$$\partial_t X(t,0) = 0 \tag{4.26}$$

which characterizes a fixed or pinned boundary, i.e., Dirichlet condition. This corresponds to a conformal boundary fixed point where the boundary operator becomes marginally relevant.

For general values of $0 < g, \bar{g} < \frac{1}{\pi}$, the system lies between the Neumann and Dirichlet limits. The boundary condition interpolates between free and pinned configurations. The critical value $|g| = 1/\pi$ thus marks a boundary phase transition between these two conformal fixed points.

This analysis situates the boundary sine-Gordon model within the broader framework of BCFT, where boundary interactions generate flows between distinct conformally

doi:10.6342/NTU202501665

invariant boundary conditions. The couplings g and $\bar{g}$ act as tunable parameters that dictate the trajectory of the boundary condition, thereby controlling physical properties such as conductance, reflection, and boundary entropy.

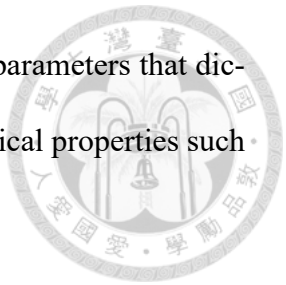

4.3.3 Dependence of Boundary Coupling on Lattice Parameter

We now explore the relationship between the boundary coupling g in the continuum theory and the microscopic hopping amplitude v in the lattice model. Starting from the parametrization derived earlier Eq. (4.18), we focus on the Hermitian case, where $v = \bar{v}^\dagger$. This implies that both g and $\bar{g}$ are real and satisfy:

$$|g| = |\bar{g}| = \frac{1}{\pi} \cdot \frac{2|v|t_0}{t_0^2 + |v|^2}$$

This expression establishes a clear, though nonlinear, map between the lattice boundary parameter $|v|$ and the effective continuum boundary coupling $|g|$. It reflects how the microscopic strength of boundary transmission governs the emergent interaction in the boundary conformal field theory. To visualize this mapping, we plot $|T^+_{k=\pi/2}|^2 = (\pi|g|)^2$ as a function of $|v|$, with fixed t, in Fig. 4.4: The plot confirms that the maximal value of $|g| = 1/\pi$ is achieved when $|v| = t_0$, corresponding to the conformal boundary point where the boundary operator is marginal. For $|v| < t_0$, the coupling $|g|$ is subcritical and the system flows towards a Neumann-like boundary condition. Conversely, for $|v| > t_0$, the effective coupling again decreases, reflecting the non-invertibility of the map: a given $|g|$ corresponds to two distinct values of $|v|$, lying on either side of the critical point. This non-uniqueness suggests that the gluing matrix U and hence the full structure of the boundary state cannot be captured solely by $|g|$; the phase information in v is essential, particularly when extended to non-Hermitian or complex v.

doi:10.6342/NTU202501665

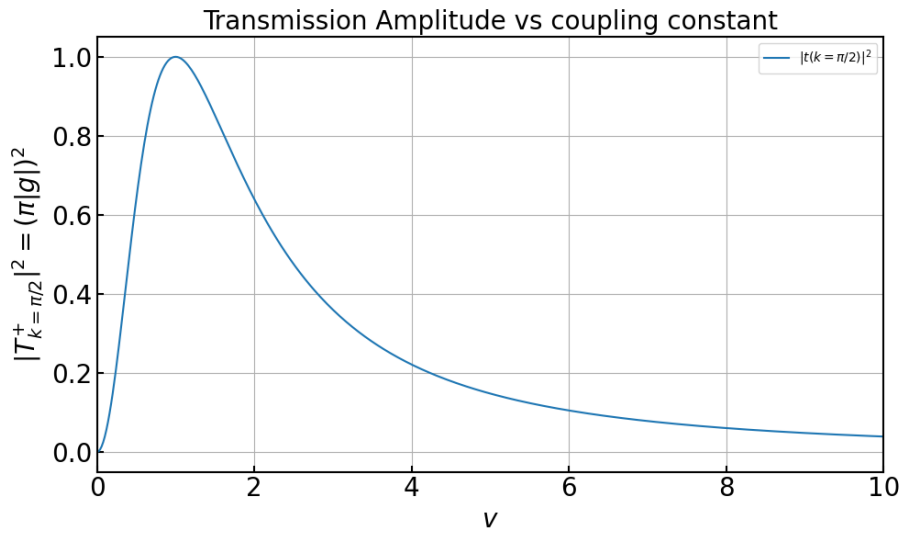

Figure 4.4: Mapping between the lattice boundary parameter $|v|$ and the transmission amplitude $|T^{+}_{k=\pi/2}|^2 = (\pi|g|)^2$. The maximum value $|g| = 1/\pi$ occurs at $|v| = t$, corresponding to the conformal boundary fixed point.

From the general gluing condition Eq. (3.37):

$$\left(\psi_R(0,\sigma) + i\sigma^1 U \psi_L(0,\sigma)\right)|BD\rangle = 0$$

we conclude that the boundary condition, and hence the boundary dynamics, depend on the full structure of U, not just its eigenvalues. Therefore, while the mapping $v \mapsto g$ captures the magnitude of the coupling, it does not uniquely fix the boundary state without further specification. In the following, we will explore several special cases to further understand the structure of this map and its implications for transport behavior.

4.3.4 Dirichlet Boundary Condition

From the general mapping between the lattice and continuum parameters, we find that the Dirichlet boundary condition corresponds to the defect-free case on the lattice.

doi:10.6342/NTU202501665

Specifically, when the hopping amplitudes are unity,

$$v = \bar{v} = t_0 \quad \Rightarrow \quad g = \bar{g} = \frac{1}{\pi} \tag{4.27}$$

the boundary interaction reaches the critical strength required to pin the field at the boundary. This corresponds to the Dirichlet fixed point in boundary conformal field theory, where the field value is fixed at the boundary.

In the fermionic formulation, the Dirichlet boundary state $|DD\rangle$ is defined by the standard gluing condition:

$$\left(\psi_R(0,\sigma) - \psi_L(0,\sigma)\right)|DD\rangle = 0 \quad , \quad \left(\psi_R^\dagger(0,\sigma) + \psi_L^\dagger(0,\sigma)\right)|DD\rangle = 0 \tag{4.28}$$

which agrees with Eq. (3.32). This condition enforces total reflection with a fixed phase, indicating that the boundary does not permit any net flow of excitations.

Under this condition, the scattering matrix becomes trivial:

$$S_k = \begin{pmatrix} 1 & 0 \\ 0 & 1 \end{pmatrix}$$

indicating that incoming modes are fully reflected without any phase shift or mixing—consistent with a perfectly reflective (Dirichlet) boundary. This result serves as a consistency check for both the fermionic and bosonic formulations, affirming that the critical coupling $g = 1/\pi$ corresponds precisely to the Dirichlet boundary condition in the BCFT description.

doi:10.6342/NTU202501665

4.3.5 Neumann Boundary Condition

The Neumann boundary condition corresponds to the decoupled limit in the lattice model, where the boundary either becomes an infinitely strong barrier or vanishes entirely:

$$v = \bar{v} \to 0 \text{ or } \infty \quad \Rightarrow \quad g = \bar{g} = 0 \tag{4.29}$$

In this regime, the boundary sine-Gordon interaction vanishes, and the field satisfies a free (Neumann-type) boundary condition. In the fermionic representation, the corresponding boundary state $|ND\rangle$ is characterized by the gluing condition:

$$\left(\psi_R(0,\sigma) + i\sigma^1\psi_L(0,\sigma)\right)|ND\rangle = 0 \quad , \quad \left(\psi_R^\dagger(0,\sigma) + \psi_L^\dagger(0,\sigma)i\sigma^1\right)|ND\rangle = 0 \tag{4.30}$$

in agreement with Eq. (3.33). This condition describes perfect transmission through the boundary up to a unitary transformation, consistent with a free boundary with no interaction potential.

In this case, the scattering matrix reduces to:

$$S_k = \begin{pmatrix} 0 & -1 \\ 1 & 0 \end{pmatrix}$$

which reflects the maximal transmission and complete exchange of left- and right-moving modes at the boundary, modulo a sign. This form captures the essential feature of the Neumann condition: zero reflection and full mode transfer across the boundary.

Together with the Dirichlet case, this establishes the two conformal fixed points in the boundary governed by the sine-Gordon interaction: Neumann and Dirichlet, with the

doi:10.6342/NTU202501665

boundary coupling g serving as the parameter.

The analysis above illustrates the boundary flow from the Neumann to Dirichlet fixed point as the boundary coupling evolves: $g = \bar{g} \in \left[0, \frac{1}{\pi}\right]$. This flow corresponds to a continuous deformation from a free (unconstrained) boundary to one where the field is maximally pinned. Within the fermionic formulation, this family of boundary conditions can be related by global $SU(2) \subset SL(2, \mathbb{C})$ transformations acting on the left-moving sector. A canonical example is:

$$|DD\rangle = e^{-i\pi J_L^1}|ND\rangle$$

where J_L^1 is a generator of the left-moving Kac-Moody algebra. This structure reflects the symmetry of the model and the exact marginality of the boundary sine-Gordon interaction at critical coupling.

4.4 Unitarity, Hermiticity, and Their Violations

A central theme in the correspondence between lattice models and BCFT is the interplay between Hermiticity and unitarity, and how their presence or violation manifests in both frameworks.

doi:10.6342/NTU202501665

4.4.1 Hermiticity in the Lattice Model

In the lattice description, the condition for Hermiticity of the Hamiltonian is straightforward. Consider the tight-binding model with a single impurity at the origin:

$$H = t_0 \sum_{i\neq 0}(c_i^\dagger c_{i+1} + h.c.) + v c_0^\dagger c_1 + \bar{v} c_1^\dagger c_0 = t_0 \sum_{i\neq 0}(c_i^\dagger c_{i+1} + h.c.) + v^\dagger c_1^\dagger c_0 + \bar{v}^\dagger c_0^\dagger c_1 = H^\dagger \tag{4.31}$$

To ensure that $H = H^\dagger$, we require the boundary couplings to satisfy:

$$v = \bar{v}^\dagger \tag{4.32}$$

This defines the Hermitian subspace of the coupling parameter space. In this case, the impurity model remains physically conservative, with no net gain or loss of probability amplitude. Under the Hermitian condition, the corresponding scattering matrix at $k = \pi/2$ simplifies to:

$$S_{k=\pi/2} = \begin{pmatrix} \dfrac{2vt_0}{t_0^2+|v|^2} & -\dfrac{t_0^2-|v|^2}{t_0^2+|v|^2} \\ \dfrac{t_0^2-|v|^2}{t_0^2+|v|^2} & \dfrac{2v^* t_0}{t_0^2+|v|^2} \end{pmatrix} \tag{4.33}$$

One can directly verify that this matrix is unitary:

$$S_k S_k^\dagger = \mathbb{I} \tag{4.34}$$

indicating that the total probability flux is conserved. Physically, this means that the impurity is purely reflective and transmissive without any absorption or amplification, precisely what is expected for a Hermitian quantum system.

In this Hermitian setting, the unitarity of the scattering matrix implies that $S_k \in SU(2)$. This symmetry reflects the deeper chiral $SU(2)_L \times SU(2)_R$ symmetry present in

doi:10.6342/NTU202501665

the fermionic representation of the boundary conformal field theory. In particular, transformations between conformal boundary states—such as between Neumann and Dirichlet—can be realized as global $SU(2)$ rotations acting on the left-moving fermions, preserving the $SU(2)$ structure of the theory. Hence, the Hermiticity of the lattice Hamiltonian ensures unitary scattering in the microscopic model. This establishes a symmetry, respecting bridge between lattice and field, theoretic descriptions of impurity systems.

4.4.2 Unitarity Condition of the Gluing Matrix

We now examine the conditions under which the gluing matrix U, acting on the boundary fermions, remains unitary. Recall the parametrized form of U, introduced in Eq. 3.37:

$$U = \begin{pmatrix} e^{-2\pi i A}\sqrt{1-\pi^2 g\bar{g}} & -i\pi g \\ -i\pi\bar{g} & e^{2\pi i A}\sqrt{1-\pi^2 g\bar{g}} \end{pmatrix}$$

To ensure physical consistency and probability conservation at the boundary, we require that $U \in U(2)$, i.e.,

$$UU^\dagger = \mathbb{I} \tag{4.35}$$

In our consideration, $A \in \mathbb{R}$. To ensure that $UU^\dagger = \mathbb{I}$, we must impose the following conditions:

$$\bar{g} = g^*, \quad |g| \leq \frac{1}{\pi}$$

These constraints ensure that the boundary interaction remains physically acceptable and does not introduce non-unitary behavior. Violations of these conditions lead to non-Hermitian dynamics and non-unitary boundary S-matrices, which we explore further in the next section. For a complete derivation of unitarity condition, see Appendix B.

doi:10.6342/NTU202501665

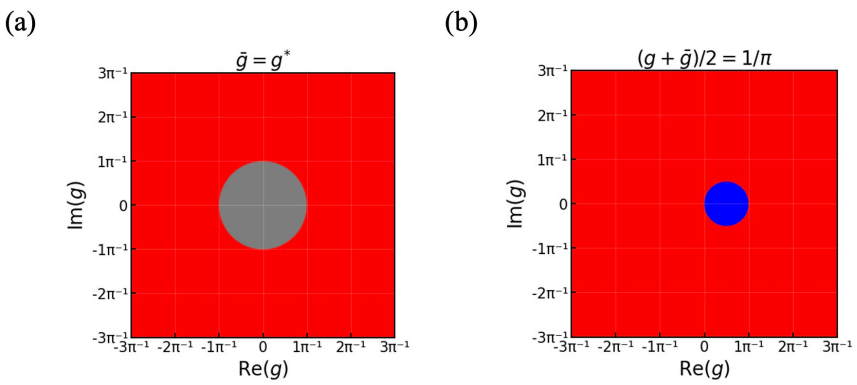

Figure 4.5: Unitarity check of the total scattering amplitude, given by $|T_F^+|^2 + |R_F^+|^2 = \pi^2|g|^2 + |1 - \pi^2 g\bar{g}|$. The blue region indicates probability loss ($|T|^2 + |R|^2 < 1$), while the red region indicates probability gain ($|T|^2 + |R|^2 > 1$). The gray region corresponds to unitarity, where total probability is conserved ($|T|^2 + |R|^2 = 1$). (a) Example with $\bar{g} = g^*$, which preserves unitarity when $|g| \leq 1/\pi$. (b) Example with $(g + \bar{g})/2 = 1/\pi$, exhibiting both probability loss and gain in different regions of the parameter space.

4.4.3 Equivalence of Unitarity and Hermiticity

To establish the correspondence between the unitarity of the boundary gluing condition in BCFT and the Hermiticity of the lattice impurity Hamiltonian, we begin by recalling the Hermiticity condition for the tight-binding model:

$$v = \bar{v}^* \tag{4.36}$$

Using the parameterization of boundary couplings in terms of the lattice variables Eq. (4.18):

$$\bar{g} = \frac{1}{\pi} \cdot \frac{2vt_0}{t_0^2 + v\bar{v}}, \quad g = \frac{1}{\pi} \cdot \frac{2\bar{v}t_0}{t_0^2 + v\bar{v}}, \quad A = \frac{1}{4}$$

we find that Hermiticity implies:

$$\bar{g}^* = \frac{1}{\pi} \cdot \frac{2v^*t_0}{t_0^2 + \bar{v}^*v^*} = \frac{1}{\pi} \cdot \frac{2\bar{v}t_0}{t_0^2 + \bar{v}v} = g \tag{4.37}$$

which is one of the unitarity conditions in BCFT: $g = \bar{g}$.

doi:10.6342/NTU202501665

We also note the inequality:

$$t_0^2 + |v|^2 \geq 2t_0|v| \tag{4.38}$$

which gives:

$$|g| = |\bar{g}| = \left|\frac{1}{\pi} \cdot \frac{2vt_0}{t_0^2 + v\bar{v}}\right| \tag{4.39}$$

$$= \left|\frac{1}{\pi} \cdot \frac{2vt_0}{t_0^2 + vv^*}\right| \tag{4.40}$$

$$= \frac{1}{\pi} \cdot \frac{2|v|t_0}{t_0^2 + |v|^2} \leq \frac{1}{\pi} \tag{4.41}$$

which ensures that g lies within the unitary region of the BCFT. Thus, Hermiticity implies unitarity.

Now consider the converse: Whether unitarity implies Hermiticity. That is, if $g = \bar{g}^*$ and $|g| \leq \frac{1}{\pi}$ implies $v = \bar{v}^*$. We analyze this by considering all three cases:

$$\begin{cases} v, \bar{v} \neq 0 \\ v = 0,\ \bar{v} \neq 0 \\ v = \bar{v} = 0 \end{cases} \tag{4.42}$$

For the first case, $v, \bar{v} \neq 0$, using the inverse mapping:

$$v = \frac{1 \pm \sqrt{1 - \pi^2 g\bar{g}}}{\pi g}\, t_0, \qquad \bar{v} = \frac{1 \pm \sqrt{1 - \pi^2 \bar{g}g}}{\pi \bar{g}}\, t_0 \tag{4.43}$$

taking the complex conjugate of $\bar{v}$ gives:

$$\frac{\bar{v}^*}{t_0} = \left(\frac{1 \pm \sqrt{1 - \pi^2 \bar{g}g}}{\pi \bar{g}}\right)^* = \frac{\left(1 \pm \sqrt{1 - \pi^2 |g|^2}\right)^*}{\pi \bar{g}^*} = \frac{1 \pm \sqrt{1 - \pi^2 g\bar{g}}}{\pi g} = \frac{v}{t_0} \tag{4.44}$$

doi:10.6342/NTU202501665

note that $\sqrt{1-\pi^2 g\bar{g}} \in \mathbb{R}$ since $|g| \leq \frac{1}{\pi}$. Hence, $\bar{v}^* = v$, confirming Hermiticity.

For the second case, $v = 0, \bar{v} \neq 0$ (or vice versa), we compute:

$$\bar{g} = \frac{2t_0 v}{t_0^2 + v\bar{v}} = 0 \tag{4.45}$$

$$g = \frac{2t_0 \bar{v}}{t_0^2 + v\bar{v}} = \frac{2\bar{v}}{t_0} \neq 0 \tag{4.46}$$

so $g \neq \bar{g}^*$, violating unitarity. Contradiction.

For the third case, $v = \bar{v} = 0$:

$$\bar{g} = \frac{2t_0 v}{t_0^2 + v\bar{v}} = 0, \quad g = \frac{2t_0 \bar{v}}{t_0^2 + v\bar{v}} = 0 \tag{4.47}$$

Then:

$$g = \bar{g} = 0, \quad \Rightarrow \quad g = \bar{g}^*, \quad \text{and} \quad v = \bar{v}^* = 0$$

Unitarity holds, and Hermiticity follows.

In conclusion, the above analysis confirms that:

Unitarity in BCFT is equivalent to Hermiticity in the lattice model.

This result reinforces the deep correspondence between the boundary gluing condition in field theory and the microscopic defect Hamiltonian. It provides a direct diagnostic: violation of unitarity in the BCFT boundary condition signals the onset of non-Hermiticity in the underlying lattice system—a regime of significant physical interest, especially in the context of non-Hermitian quantum mechanics and PT-symmetric systems.

doi:10.6342/NTU202501665

4.5 Ground State Energy

We aim to extract the critical (ground-state) energy of a non-Hermitian impurity system by analyzing the structure of its scattering matrix. The underlying intuition is rooted in the correspondence between the finite-size energy spectrum and boundary conditions in CFT, where phase shifts induced by the scattering matrix lead to universal energy corrections.

Although the notion of a well-defined Fermi level generally breaks down in non-Hermitian systems due to the complex nature of the energy spectrum, we can still focus on cases where the spectrum remains real—such as those exhibiting PT-symmetry. Furthermore, we will demonstrate that near the critical point, the imaginary components of the spectrum vanish when the scattering amplitudes are real. This observation enables us to reliably extract the critical (ground-state) behavior of the non-Hermitian system.

Recall the general form of the S-matrix for the non-Hermitian system, as given in Eq. (4.10): case (4.10):

$$S_k = \begin{pmatrix} \dfrac{(1-e^{2ik})\,vt_0}{t_0^2 - v\bar{v}\,e^{2ik}} & -\dfrac{t_0^2 - v\bar{v}}{t_0^2 - v\bar{v}\,e^{2ik}} \\ -\dfrac{t_0^2 - v\bar{v}}{t_0^2 - v\bar{v}\,e^{2ik}}\,e^{2ik} & \dfrac{(1-e^{2ik})\,\bar{v}t_0}{t_0^2 - v\bar{v}\,e^{2ik}} \end{pmatrix}$$

The key idea is that the phase shift induced by boundary scattering modifies the allowed momentum quantization conditions in finite volume. For periodic systems with impurities (or equivalently, BCFT setups with boundaries), the total phase shift contributes a shift in the energy spectrum. At the conformal point $k = \pi/2$, the S-matrix simplifies (as discussed earlier), and the associated phase shift can be extracted from the eigenvalues of the S-matrix.

doi:10.6342/NTU202501665

4.5.1 Eigenvalues of S-matrix

To extract the phase shift and ground state energy from the scattering matrix, we begin by analyzing the eigenvalues of S_k. Define the determinant of the matrix as:

$$\det S_k \equiv \Delta(k, t_0, v, \bar{v}) = T_k^+ T_k^- - R_k^+ R_k^-$$

A direct calculation yields:

$$\det S_k = \frac{1}{(t_0^2 - v\bar{v}e^{2ik})^2}\left[(1-e^{2ik})^2 v\bar{v}t_0^2 - (t_0^2 - v\bar{v})^2 e^{2ik}\right] = -e^{2ik}\cdot\frac{t_0^2 - v\bar{v}e^{-2ik}}{t_0^2 - v\bar{v}e^{2ik}} \tag{4.48}$$

At the special momentum $k = \pm\pi/2$, corresponding to the critical point of the 1D lattice model, we find:

$$\Delta = \det S_{k=\frac{\pi}{2}} = -e^{2ik}\cdot\frac{t_0^2 - v\bar{v}e^{-2ik}}{t_0^2 - v\bar{v}e^{2ik}} = 1 \tag{4.49}$$

Thus, for any values of $v, \bar{v}$, the determinant satisfies:

$$\det S_{k=\pm\pi/2} = 1 \tag{4.50}$$

To obtain the eigenvalues λ, we solve the characteristic equation:

$$\det\begin{pmatrix} T_k^+ - \lambda & R_k^- \\ R_k^+ & T_k^- - \lambda \end{pmatrix} = (T_k^+ - \lambda)(T_k^- - \lambda) - R_k^- R_k^+ = 0 \tag{4.51}$$

Using the earlier definition of Δ, this becomes:

$$\lambda^2 - \lambda(T_k^+ + T_k^-) + \Delta = 0 \tag{4.52}$$

doi:10.6342/NTU202501665

with solutions:

$$\lambda_{\pm} = \frac{T_k^+ + T_k^-}{2} \pm \sqrt{\left(\frac{T_k^+ + T_k^-}{2}\right)^2 - \Delta} \tag{4.53}$$

These eigenvalues encode the complex phase shifts introduced by boundary scattering and, at $k = \pi/2$, their phases determine the momentum shift in the finite-size spectrum. From this, one can compute the ground state (critical) energy.

4.5.2 Quantization Condition

The quantization condition arises from combining the periodic boundary condition (P.B.C.) with the spectral properties of the scattering matrix S_k.

First, impose the periodic boundary condition on the folded fermions:

$$\begin{pmatrix} \tilde{\psi}_k^+ \\ \tilde{\psi}_k^- \end{pmatrix} = \begin{pmatrix} e^{ikL}\psi_k^+ \\ e^{-ikL}\psi_k^- \end{pmatrix} \quad \Rightarrow \quad \begin{pmatrix} \psi_k^+ \\ \tilde{\psi}_k^- \end{pmatrix} = e^{-ikL} \begin{pmatrix} \tilde{\psi}_k^+ \\ \psi_k^- \end{pmatrix} \tag{4.54}$$

Meanwhile, the scattering matrix connects the incoming and outgoing amplitudes as:

$$S_k \begin{pmatrix} \tilde{\psi}_k^+ \\ \psi_k^- \end{pmatrix} = \begin{pmatrix} \psi_k^+ \\ \tilde{\psi}_k^- \end{pmatrix} \tag{4.55}$$

Combining these, we obtain the quantization condition:

$$S_k \psi_{\text{in}} = e^{-ikL} \psi_{\text{in}} \tag{4.56}$$

Thus, the allowed momenta k are those for which e^{-ikL} equals an eigenvalue $\lambda_{\pm}$ of the matrix S_k:

$$e^{-ikL} = \lambda_{\pm} \tag{4.57}$$

doi:10.6342/NTU202501665

we know the eigenvalues from Eq. (4.53):

$$\lambda_{\pm} = \frac{T_k^+ + T_k^-}{2} \pm \sqrt{\left(\frac{T_k^+ + T_k^-}{2}\right)^2 - \Delta}$$

where $\Delta = \det S_k = T_k^+ T_k^- - R_k^+ R_k^-$

We now recast this expression into a more physically transparent form. Write:

$$\lambda_{\pm} = \Delta^{1/2} \left[\cos\alpha \pm i \sin\alpha\right] = \Delta^{1/2} e^{\pm i\alpha} \tag{4.58}$$

where

$$\cos\alpha = \frac{T_k^+ + T_k^-}{2\Delta^{1/2}} \tag{4.59}$$

This gives the final form of the quantization condition:

$$e^{-ikL} = \lambda_{\pm} = \Delta^{1/2} \exp\left[\pm i \arccos\left(\frac{T_k^+ + T_k^-}{2\Delta^{1/2}}\right)\right] \tag{4.60}$$

This form reveals the important physical constraints that the quantized momenta are determined by the phase of the eigenvalues of S_k, capturing how the impurity affects finite-size energy levels.

This formalism provides the gateway for computing boundary-induced spectral shifts and, ultimately, the ground state energy from the microscopic scattering data.

doi:10.6342/NTU202501665

4.5.3 Energy Spectrum Expansion

The representation of the scattering matrix eigenvalues $\lambda_\pm$ allows us to define and compute the quasi-quantum numbers q_n, which encode boundary-induced momentum shifts in a finite system. Starting from the quantization condition Eq. (4.60):

$$\lambda_\pm = \Delta^{1/2} e^{\pm i\alpha} = \Delta^{1/2} \exp\left[\pm i \arccos\left(\frac{T_k^+ + T_k^-}{2\Delta^{1/2}}\right)\right] \tag{4.61}$$

we define the quasi-momentum q_n associated with the $n-th$ level as a second-order expansion in the system size L:

$$q_n \equiv k_n + \frac{\phi_\pm(k_n)}{L} + \frac{1}{2L^2}\frac{d}{dk_n}\left[\phi_\pm(k_n)\right] + \mathcal{O}(L^{-3}), \qquad k_n = \frac{2\pi n}{L} \tag{4.62}$$

This expansion arises from solving the quantization condition perturbatively, expand $q_n = k_n + \frac{\phi_\pm(q_n)}{L}$ over the L^{-1} order, treating $\phi_\pm(k_n)$ as a momentum-dependent phase shift. For a detailed derivation, see Appendix C.

The phase shift $\phi_\pm(k_n)$ is defined from the logarithm of the eigenvalue:

$$\phi_\pm(k_n) = \ln\left[\Delta^{1/2} e^{\pm i\alpha}\right] = -i \ln \Delta^{1/2} \pm \arccos\left(\frac{T_k^+ + T_k^-}{2\Delta^{1/2}}\right) \tag{4.63}$$

Substituting the quasi-momentum $q_n^\pm$ into the dispersion relation of the system, and performing a Taylor expansion, we derive the finite-size energy spectrum:

$$E = \tilde{c}_1 L + \tilde{c}_0 + \tilde{c}_{-1} L^{-1} + \mathcal{O}(L^{-2}) \tag{4.64}$$

where the coefficients $\tilde{c}_1, \tilde{c}_0, \tilde{c}_{-1}$ are determined by the dispersion relation and the phase shift $\phi_\pm(k_n)$. In particular: $\tilde{c}_1$ reflects the bulk ground state energy density, $\tilde{c}_0$ contains

doi:10.6342/NTU202501665

non-universal boundary contributions, $\tilde{c}_{-1}$ captures universal scaling corrections from boundary phase shifts, related to the BCFT via $E_0 = \delta^2 - \frac{1}{12}$.

This formalism offers a powerful method to compute boundary-modified finite-size energy levels directly from the microscopic scattering matrix, establishing a direct bridge between the lattice impurity problem and the continuum BCFT description.

We now compute the finite-size ground-state energy E_{GS} by expanding the lattice dispersion relation in terms of the quasi-momenta $q_n^{\pm}$. Due to the presence of the impurity, the energy spectrum becomes split between two sectors. Without loss of generality, we assume $\arccos\left(\frac{T_F^+ + T_F^-}{2}\right) \geq 0$, which allows us to assign the impurity-induced phase shift ϕ_- to right-moving particles, and ϕ_+ to left-moving particles. The total ground-state energy is then computed by summing the energy contributions of all occupied states within the band:

$$E_{GS} = 2t_0 \sum_{n=-\ell}^{0} \cos(q_n^+) + 2t_0 \sum_{n=1}^{\ell} \cos(q_n^-) = \tilde{c}_1 L + \tilde{c}_0 + \tilde{c}_{-1} L^{-1} + \mathcal{O}(L^{-2}) \tag{4.65}$$

where the quasi-momenta $q_n^{\pm}$ are expanded as:

$$\cos(q_n^{\pm}) = \cos\left(k_n + \frac{\phi_{\pm}(k_n)}{L} + \frac{1}{2L^2}\frac{d}{dk_n}\left[\phi_{\pm}(k_n)^2\right] + \mathcal{O}(L^{-3})\right) \tag{4.66}$$

Expanding to L^{-2} order:

$$\cos(q_n^{\pm}) = \cos k_n \cos\left(\frac{\phi_{\pm}}{L} + \frac{1}{2L^2}\frac{d}{dk_n}\phi_{\pm}^2 + \cdots\right) - \sin k_n \sin\left(\frac{\phi_{\pm}}{L} + \frac{1}{2L^2}\frac{d}{dk_n}\phi_{\pm}^2 + \cdots\right) \tag{4.67}$$

doi:10.6342/NTU202501665

Thus,

$$\cos(q_n^{\pm}) = \underbrace{\cos k_n}_{\tilde{c}_1 L} - \underbrace{\sin k_n \frac{\phi_{\pm}}{L}}_{\tilde{c}_0} - \underbrace{\frac{1}{2L^2}\left(\frac{d}{dk_n}\left[\sin k_n \phi_{\pm}^2\right]\right)}_{\tilde{c}_{-1}L^{-1}} + \mathcal{O}(L^{-3}) \tag{4.68}$$

Putting the expansion for $\cos(q_n^{\pm})$ from Eq. (4.68) back into the total energy expression Eq.(4.65), we identify the individual contributions to the finite-size energy expansion:

$$E_c = 2t_0 \sum_{n=-\ell}^{0} \cos(q_n^{+}) + 2t_0 \sum_{n=1}^{\ell} \cos(q_n^{-}) = \tilde{c}_1 L + \tilde{c}_0 + \tilde{c}_{-1} L^{-1} + \mathcal{O}(L^{-2})$$

with each term arising as follows:

Leading extensive term $\tilde{c}_{+1}$ arises from the unshifted dispersion:

$$\tilde{c}_{+1} = \frac{2t_0}{L}\left(\sum_{n=-\ell}^{0} \cos k_n + \sum_{n=1}^{\ell} \cos k_n\right) = \sum_{n=-\ell}^{\ell} \cos k_n \tag{4.69}$$

Where we know,

$$\tilde{c}_{+1} = \frac{2t_0}{L}\frac{\sin(\frac{2\ell+1}{L})}{2\sin(\frac{\pi}{L})} = \frac{2t_0 \sin k_F}{\pi} + \frac{2t_0 \pi \sin k_F}{6L^2} + + \mathcal{O}(L^{-3}) = -\frac{v_F}{\pi} - \frac{\pi v_F}{6L^2} + \mathcal{O}(L^{-3}) \tag{4.70}$$

with $k_F = \frac{\pi}{2}, \quad v_F = -2t_0 \sin k_F$ which corresponds to the bulk ground state energy.

Next-to-leading correction $\tilde{c}_0$ captures boundary-induced shifts due to the first-order phase shift:

$$\tilde{c}_0 = -\frac{2t_0}{L}\left(\sum_{n=-\ell}^{0} \sin k_n \, \phi_+ + \sum_{n=1}^{\ell} \sin k_n \, \phi_-\right) \tag{4.71}$$

$$= -\frac{2t_0}{L}\frac{L}{2\pi}\left(\int_{-k_F}^{0} dk \, \sin k \, \phi_+ + \int_{0}^{k_F} dk \, \sin k \, \phi_-\right) \tag{4.72}$$

$$= -\frac{t_0}{\pi}\int_{0}^{k_F} \left[\phi_-(k) - \phi_+(-k)\right] \sin k \, dk \tag{4.73}$$

doi:10.6342/NTU202501665

Here, we replaced the discrete sum $\sum_n$ with an integral via $\sum_n \to \frac{L}{2\pi}\int dk$, noting that $k_n = \frac{2\pi n}{L} \Rightarrow dk = \frac{2\pi}{L}dn$. The value of $\tilde{c}_0$ depends only on the microscopic parameters $t_0, v, \bar{v}$, not on the system size.

Finite-size universal term $\tilde{c}_{-1}$ includes contributions from second-order shifts:

$$\tilde{c}_{-1} = -\frac{2t_0}{2L}\left(\sum_{n=-\ell}^{0}\frac{d}{dk_n}\sin k_n\,\phi_+^2 + \sum_{n=1}^{\ell}\frac{d}{dk_n}\sin k_n\,\phi_-^2\right) \tag{4.74}$$

$$= \frac{v_F}{2\pi}\left(\arccos\left(\frac{T^+ + T^-}{2\Delta^{1/2}}\right)^2 + \left(i\ln\Delta^{1/2}\right)^2\right) + \mathcal{O}(L^{-1}) \tag{4.75}$$

which directly reproduces the conformal energy shift predicted by BCFT. The second term in this expression arises from the logarithmic branch cut of the determinant and encodes the non-Hermitian contribution to the energy spectrum.

Moreover, the sub-leading correction originally appearing in the c_1 expansion as $\frac{\pi v_F}{6L^2}$, which represents the vacuum energy contribution from the bulk, also contributes at $O(L^{-1})$ and must be incorporated into c_{-1}. Therefore, we refine the expression for the finite-size correction term:

$$\tilde{c}_{-1} = \frac{v_F}{2\pi}\cdot\arccos\left(\frac{T_F^+ + T_F^-}{2}\right)^2 - \frac{\pi v_F}{6} \tag{4.76}$$

This final form explicitly isolates the universal boundary contribution to the ground state energy, with the first two terms capturing the full effect of the boundary scattering phase shift and the last term subtracting the bulk vacuum energy in accordance with the standard result for CFT theory on an interval.

This expansion robustly demonstrates that the low-energy spectrum of a 1D system with a boundary impurity is governed by the complex phase shifts encoded in the eigen-

doi:10.6342/NTU202501665

values of the S-matrix, providing a bridge between microscopic lattice models and their BCFT descriptions.

4.5.4 Matching Finite-Size Corrections to BCFT Predictions

Recall the parameterization connecting the microscopic boundary hopping amplitude v with the continuum sine-Gordon couplings: remember the parameterization Eq. (4.18):

$$\bar{g} = \frac{1}{\pi} \cdot \frac{2vt_0}{t_0^2 + v\bar{v}}, \quad g = \frac{1}{\pi} \cdot \frac{2\bar{v}t_0}{t_0^2 + v\bar{v}}, \quad A = \frac{1}{4}$$

with Eq. (4.17):

$$\mathcal{S}_{k=\pi/2} = i\sigma^1 U$$

The corresponding boundary partition function $Z_{BD}(\beta)$, encoding the exact energy spectrum including finite-size effects, is given by Eq. (3.42):

$$Z_{BD}(\beta) = e^{\frac{\beta}{24}} \sum_n e^{-\beta(n+\delta)^2} \prod_{k=1}^{\infty} \frac{1}{1 - e^{-\beta k}}$$

where the spectral shift δ is determined by the boundary interaction:

$$\delta = \frac{1}{2\pi} \cos^{-1}\left(\frac{\pi}{2}(g + \bar{g})\right) \tag{4.77}$$

Using the parameterization above, this becomes:

$$\delta = \frac{1}{2\pi} \cos^{-1}\left(\frac{T_F^+ + T_F^-}{2}\right) \tag{4.78}$$

where $T_F^{\pm}$ are the diagonal transmission amplitudes in the scattering matrix evaluated at the Fermi point $k_F = \pi/2$

doi:10.6342/NTU202501665

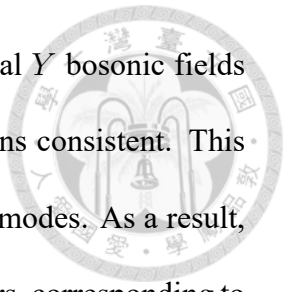

However, in the fermionic representation, both the X and its dual Y bosonic fields must be included to ensure that the total conformal dimension remains consistent. This duality reflects the need to account for both momentum and winding modes. As a result, the full partition function should be written as the product of two sectors, corresponding to the sum of Ramond (R) and Neveu-Schwarz (NS) representations of the fermionic field:

$$Z_{tot} = Z_R + Z_{NS} = Z_X \cdot Z_Y \tag{4.79}$$

$$= \left(e^{\frac{\beta}{24}} \sum_n e^{-\beta(n+\delta)^2} \prod_{k=1}^{\infty} \frac{1}{1-e^{-\beta k}} \right) \left(e^{\frac{\beta}{24}} \sum_n e^{-\beta n^2} \prod_{k=1}^{\infty} \frac{1}{1-e^{-\beta k}} \right) \tag{4.80}$$

The corresponding energy levels take the form:

$$E_{m,n} = m^2 + (n+\delta)^2 + N - \frac{1}{12} \tag{4.81}$$

and the ground state energy is:

$$E_0 = \delta^2 - \frac{1}{12} = \left(\frac{1}{2\pi} \cos^{-1} \left(\frac{T_F^+ + T_F^-}{2} \right) \right)^2 - \frac{1}{12} \tag{4.82}$$

From the lattice analysis, the L^{-1} term in the finite-size energy expansion is:

$$\tilde{c}_{-1} L^{-1} = \left(\frac{v_F}{2\pi} \left[\cos^{-1} \left(\frac{T_F^+ + T_F^-}{2} \right) \right]^2 - \frac{\pi v_F}{6} \right) L^{-1} \tag{4.83}$$

Comparing this to the BCFT prediction, we find perfect agreement:

$$\tilde{c}_{-1} L^{-1} = \frac{2\pi v_F}{L} E_0 \tag{4.84}$$

Here, the term $-\frac{\pi v_F}{6L}$ represents the universal vacuum (Casimir) energy of the Tomonaga–Luttinger liquid, corresponding to the central charge $c = 2$ in the conformal field the-

doi:10.6342/NTU202501665

ory description. In the presence of an impurity, an additional finite-size correction arises due to the scattering phase shift δ, which modifies the boundary condition of the system. This phase shift contributes an additive term proportional to δ^2, as captured in the total energy via:

$$E_{imp} = \frac{v_F}{2\pi L}\left[\cos^{-1}\left(\frac{T_F^+ + T_F^-}{2}\right)\right]^2 = \frac{2\pi v_F}{L}\delta^2. \tag{4.85}$$

This matching establishes a precise equivalence between the boundary finite-size energy corrections derived from the microscopic impurity model and the universal spectral shifts predicted by BCFT. It underscores how the phase structure of the scattering matrix fully encodes the low-energy physics, including boundary interactions, spectral flow, and so on. Importantly, this correspondence extends beyond Hermitian systems: it provides a powerful framework for predicting the behavior of non-Hermitian quantum systems using BCFT techniques.

4.6 Excited State Energy

In the previous section, we argued that the ground state energy of the BCFT may correspond to the half-filling critical energy of the non-Hermitian impurity system. Given that the energy spectrum of the BCFT, as expressed in Eq. (4.81), includes excited states of the form:

$$E_{m,n} = m^2 + (n+\delta)^2 + N - \frac{1}{12}$$

an important question arises: do these excited energies correspond to those of the non-Hermitian impurity system, and what is their physical interpretation? To address this question, we must compute the excited-state energy spectrum of our system.

doi:10.6342/NTU202501665

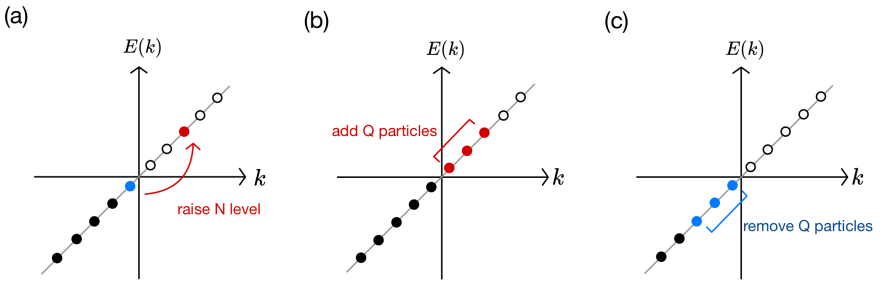

Figure 4.6: Illustration of typical excitations in the system: (a) Promotion of a particle by N energy levels. (b) adding Q particles. (c) removing Q particles. The horizontal axis represents momentum k near the Fermi point k_F, while the vertical axis denotes the energy $E(k)$ near the Fermi energy E_F. Solid dots indicate occupied energy levels, and hollow dots represent unoccupied levels. Blue and red dots correspond to particle removal and addition, respectively.

4.6.1 Excitations by Raising N Levels

First, we recall the expression for the critical energy of our system, given in Eq.(4.65):

$$E_{GS} = 2t_0 \sum_{n=-\ell}^{0} \cos(q_n^+) + 2t_0 \sum_{n=1}^{\ell} \cos(q_n^-) = \tilde{c}_1 L + \tilde{c}_0 + \tilde{c}_{-1} L^{-1} + \mathcal{O}(L^{-2})$$

where the critical state is defined at half-filling, implying the Fermi momentum is $k_F^{\pm} = \pm\pi/2$. To compute the energy of an excited state formed by promoting the $i-th$ particle by N_i levels near the Fermi point, as illustrated in Fig.4.6(a), we use:

$$E_N = \sum_i 2t_0 \cos(q_i') - 2t_0 \cos(q_i) \tag{4.86}$$

To analyze this expression, we expand the dispersion relation around the quantized momenta:

$$\begin{aligned} \cos(q_n^{\pm}) &= \cos\left(k_n + \frac{\phi_{\pm}(k_n)}{L} + \frac{1}{2L^2}\frac{d}{dk_n}\left[\phi_{\pm}(k_n)^2\right] + \mathcal{O}(L^{-3})\right) \\ &= \cos k_n - \sin k_n \frac{\phi_{\pm}}{L} - \frac{1}{2L^2}\frac{d}{dk_n}\left(\sin k_n \phi_{\pm}^2\right) + \mathcal{O}(L^{-3}) \end{aligned} \tag{4.87}$$

doi:10.6342/NTU202501665

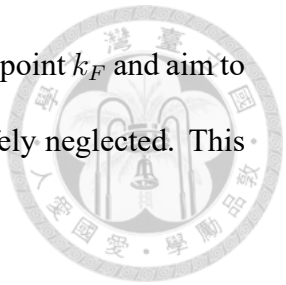

However, since we are only considering a few particles near the Fermi point k_F and aim to evaluate terms up to order L^{-1}, higher order contributions can be safely neglected. This leads to the simplified expansion:

$$\cos(q_n^{\pm}) \approx \cos k_n - \sin k_n \frac{\phi_{\pm}(k_n)}{L} + \mathcal{O}(L^{-2}) \tag{4.88}$$

Therefore, the energy difference for a single particle promoted from q_i to q_i' becomes:

$$\cos(q_i') - \cos(q_i) = \left(\cos k_n' - \sin k_n' \frac{\phi_{\pm}(k_n')}{L}\right) - \left(\cos k_n - \sin k_n \frac{\phi_{\pm}(k_n)}{L}\right) \tag{4.89}$$

where k_i and k_i' denote the quantized momenta before and after excitation, respectively.

We now expand around the Fermi point $k_F^{\pm} = \pm\pi/2$, using the quantization relation $k_n = k_F^{\pm} \pm \frac{2\pi\ell}{L}$. The cosine term becomes:

$$\begin{aligned}
\cos(k_n) &= \cos(k_F^{\pm} \pm \frac{2\pi\ell}{L}) \\
&= \cos k_F^{\pm} \cos(\frac{2\pi\ell}{L}) \mp \sin k_F^{\pm} \sin(\frac{2\pi\ell}{L}) \\
&\approx \mp \sin k_F^{\pm} \cdot \frac{2\pi\ell}{L} + \mathcal{O}(L^{-3})
\end{aligned} \tag{4.90}$$

where we have used $\cos k_F^{\pm} = \cos(\pm\pi/2) = 0$, and expanded $\sin\left(\frac{2\pi\ell}{L}\right) \approx \frac{2\pi\ell}{L}$ to leading order.

Similarly, for the sine term:

$$\begin{aligned}
\sin(k_n) &= \sin(k_F^{\pm} \pm \frac{2\pi\ell}{L}) \\
&= \sin k_F^{\pm} \cos(\frac{2\pi\ell}{L}) \pm \cos k_F^{\pm} \sin(\frac{2\pi\ell}{L}) \\
&\approx \sin k_F^{\pm} + \mathcal{O}(L^{-2})
\end{aligned} \tag{4.91}$$

doi:10.6342/NTU202501665

where $\cos(k_F^{\pm}) = 0$ and $\cos\left(\pm\frac{2\pi\ell}{L}\right) \approx 1$.

For the scattering phase factor, we expand:

$$\frac{\phi_{\pm}(k_n)}{L} = \frac{1}{L}\phi_{\pm}(k_F^{\pm} \pm \frac{2\pi\ell}{L}) \approx \frac{1}{L}\phi_{\pm}(k_F^{\pm}) + \mathcal{O}(L^{-2}) \tag{4.92}$$

Thus, we have:

$$\begin{aligned}
\cos(q_i') - \cos(q_i) &= \left(\cos k_n' - \sin k_n' \frac{\phi_{\pm}(k_n')}{L}\right) - \left(\cos k_n - \sin k_n \frac{\phi_{\pm}(k_n)}{L}\right) \\
&= \left[\mp \sin k_F^{\pm} \cdot \frac{2\pi\ell_i'}{L} - \sin k_F^{\pm} \cdot \frac{1}{L}\phi_{\pm}(k_F^{\pm})\right] \\
&- \left[\mp \sin k_F^{\pm} \cdot \frac{2\pi\ell_i}{L} - \sin k_F^{\pm} \cdot \frac{1}{L}\phi_{\pm}(k_F^{\pm})\right] \\
&= \mp \sin k_F^{\pm} \cdot \frac{2\pi(\ell_i' - \ell_i)}{L} \\
&= \mp \sin k_F^{\pm} \cdot \frac{2\pi N_i}{L}
\end{aligned} \tag{4.93}$$

where $N_i = \ell_i$' $- \ell_i$ denotes the number of levels by which the $i-th$ particle is promoted.

The total excitation energy then becomes:

$$\begin{aligned}
E_N &= \sum_i \left[2t_0 \cos(q_i') - 2t_0 \cos(q_i)\right] \\
&= \sum_i 2t_0 \left[\mp \sin k_F^{\pm} \cdot \frac{2\pi N_i}{L}\right] \\
&= \frac{2\pi v_F}{L} \sum_i N_i
\end{aligned} \tag{4.94}$$

where we have defined the Fermi velocity as $v_F = -2t_0 \sin k_F$, and

$$N_i \in \mathbb{N}_0 \quad \Rightarrow \quad \sum_i N_i \in \mathbb{N}_0 \tag{4.95}$$

This result implies that the excitation energies are non-negative relative to the ground state.

doi:10.6342/NTU202501665

Consequently, these excitations may correspond to the $N-th$ excited states in the BCFT spectrum, with degeneracy $p[N]$.

4.6.2 Excitations by Adding or Removing Q Particles

We have identified the physical interpretation of one class of excitation numbers. To explore another, we now compute the energy of an excited state formed by adding or removing Q particles to the ground state.

Note that ℓ can take either integer or half-integer values, corresponding to periodic and anti-periodic boundary conditions, respectively, as shown in Fig. 4.7. This distinction reflects the underlying fermionic parity sector and influences the allowed momentum quantization in the finite-size system.

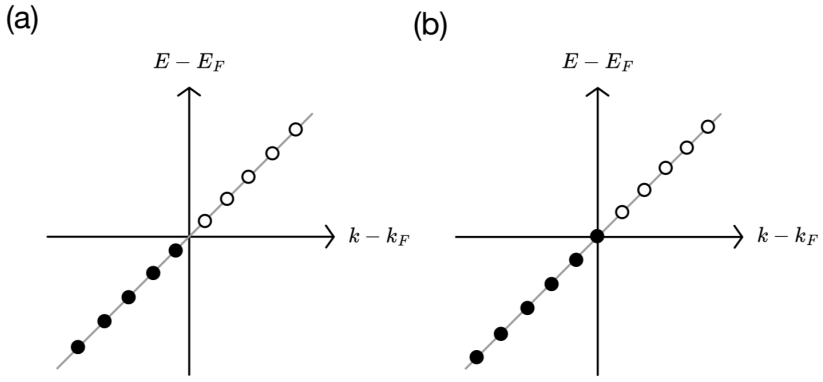

Figure 4.7: Free fermion energy levels with different periodic condition: (a) anti-periodic boundary condition, corresponds to half-integer ℓ. (b) periodic boundary condition, corresponds to integer ℓ.

First we consider the anti-periodic one (half integer). To analyze the excitation resulting from adding Q particles to the ground state, we denote the corresponding energy variation as ΔE_Q^+. This energy arises from summing the contributions of the additional Q

doi:10.6342/NTU202501665

particles placed just above the Fermi point:

$$\Delta E_Q^+ = 2t_0 \sum_{\ell=\frac{1}{2}}^{Q-\frac{1}{2}} \cos(q_n^\pm) \tag{4.96}$$

$$\begin{aligned}
&= 2t_0 \sum_{\ell=\frac{1}{2}}^{Q-\frac{1}{2}} \left[\cos k_n - \sin k_n \frac{\phi_\pm(k_n)}{L} + \mathcal{O}(L^{-2})\right] \\
&= 2t_0 \sum_{\ell=\frac{1}{2}}^{Q-\frac{1}{2}} \left[\mp \sin k_F^\pm \cdot \frac{2\pi\ell}{L} - \sin k_F^\pm \cdot \frac{1}{L}\phi_\pm(k_F^\pm) + \mathcal{O}(L^{-2})\right] \\
&= \mp 2t_0 \sin k_F^\pm \sum_{\ell=\frac{1}{2}}^{Q-\frac{1}{2}} \left[\frac{2\pi\ell}{L} \pm \frac{1}{L}\phi_\pm(k_F^\pm) + \mathcal{O}(L^{-2})\right] \\
&= \frac{v_F}{L}\left[2\pi\frac{Q^2}{2} \pm Q\phi_\pm(k_F^\pm)\right], \quad Q \in \mathbb{N}
\end{aligned} \tag{4.97}$$

where we used the definition $v_F = -2t_0 \sin k_F$, and the fact that $\sum_{\ell=\frac{1}{2}}^{Q-\frac{1}{2}} \ell = \frac{Q^2}{2}$.

Similarly, for the case of removing Q particles from the ground state, we denote the corresponding energy variation as ΔE_Q^-. This energy results from summing the contributions of the removed particles, which were initially located just below the Fermi point. Here, the momenta are given by $k_n = k_F - \frac{2\pi\ell}{L}$. The energy shift is:

$$\Delta E_Q^- = -2t_0 \sum_{\ell=\frac{1}{2}}^{Q-\frac{1}{2}} \cos(q_n^\pm) \tag{4.98}$$

$$\begin{aligned}
&= -2t_0 \sum_{\ell=\frac{1}{2}}^{Q-\frac{1}{2}} \left[\cos k_n - \sin k_n \frac{\phi_\pm(k_n)}{L} + \mathcal{O}(L^{-2})\right] \\
&= -2t_0 \sum_{\ell=\frac{1}{2}}^{Q-\frac{1}{2}} \left[\pm \sin k_F^\pm \cdot \frac{2\pi\ell}{L} - \sin k_F^\pm \cdot \frac{1}{L}\phi_\pm(k_F^\pm) + \mathcal{O}(L^{-2})\right] \\
&= \mp 2t_0 \sin k_F^\pm \sum_{\ell=\frac{1}{2}}^{Q-\frac{1}{2}} \left[\frac{2\pi\ell}{L} \mp \frac{1}{L}\phi_\pm(k_F) + \mathcal{O}(L^{-2})\right] \\
&= \frac{v_F}{L}\left[2\pi\frac{Q^2}{2} \mp Q\phi_\pm(k_F)\right], \quad Q \in \mathbb{N}
\end{aligned} \tag{4.99}$$

doi:10.6342/NTU202501665

This analysis reveals that the additive energy expression for removing Q particles mirrors that for adding Q particles when we analytically continue the result by mapping $Q \to -Q$. Consequently, we can unify the two cases into a single expression:

$$\Delta E_Q = \frac{v_F}{L}\left[2\pi\frac{Q^2}{2} \pm Q\phi_\pm(k_F^\pm)\right], \quad Q \in \mathbb{Z} \tag{4.100}$$

This unified form captures the energy variation due to half-integer valued charge excitations Q, whether positive (addition) or negative (removal), and aligns naturally with the BCFT picture of charge sector quantization.

For the case of adding (or removing) Q_R/Q_L particles in the left/right sectors, respectively, the total excitation energy becomes:

$$E_Q = \frac{v_F}{L}\left[2\pi\frac{Q_R^2}{2} + Q_R\phi_+(k_F) + 2\pi\frac{Q_L^2}{2} - Q_L\phi_-(k_F^-)\right] \tag{4.101}$$

Recall the expression for $\phi_\pm(k_n)$ from Eq. (4.63):

$$\phi_\pm(k_n) = \ln\left[\Delta^{1/2}e^{\pm i\alpha}\right] = -i\ln\Delta^{1/2} \pm \arccos\left(\frac{T_k^+ + T_k^-}{2\Delta^{1/2}}\right)$$

We define the effective phase shift at the Fermi point as:

$$\phi_F \equiv \frac{1}{2}\left[\phi_+(k_F^\pm) - \phi_-(k_F^\pm)\right] = \arccos\left(\frac{T_F^+ + T_F^-}{2}\right) \tag{4.102}$$

Substituting this into the energy expression yields:

$$E_Q = \frac{2\pi v_F}{L}\left[\frac{Q_R^2}{2} + \frac{Q_L^2}{2}\right] + \frac{v_F}{L}(Q_R - Q_L)\phi_F \tag{4.103}$$

doi:10.6342/NTU202501665

In summary, the total excitation energy can be expressed as:

$$E = E_{GS} + E_N + E_Q \tag{4.104}$$

where the contributions are:

$$E_N = \frac{2\pi v_F}{L} \sum_i N_i \tag{4.105}$$

and E_Q as derived previously accounts for the charge-sector excitations.

Furthermore, the finite-size correction at order L^{-1} to the critical energy is given by:

$$\tilde{c}_{-1} L^{-1} = \left(\frac{v_F}{2\pi} \phi_F^2 - \frac{\pi v_F}{6} \right) L^{-1} \tag{4.106}$$

which matches the expected structure from boundary conformal field theory, including the universal Casimir energy and impurity-induced phase shift contributions.

4.6.3 Correspondence Between Excitation Energies and BCFT Spectrum

We now consider the L^{-1} correction to the total excited-state energy. Combining all previously derived contributions, the finite-size corrected excitation energy takes the form:

$$E_{-1} = \frac{v_F}{L} \left(\frac{1}{2\pi} \phi_F^2 + 2\pi \left[\frac{Q_R^2}{2} + \frac{Q_L^2}{2} \right] + (Q_R - Q_L)\phi_F \right) + \frac{2\pi v_F}{L} \sum_i N_i - \frac{\pi v_F}{6L} \tag{4.107}$$

where the final term represents the universal Casimir energy contribution.

doi:10.6342/NTU202501665

Recall the excited-state energy in BCFT, as given in Eq. (4.81):

$$E_n = m^2 + (n+\delta)^2 + N - \frac{1}{24}$$

where the shift δ is determined by the boundary scattering phase:

$$\delta = \frac{1}{2\pi}\cos^{-1}\left(\frac{T_F^+ + T_F^-}{2}\right) = \frac{1}{2\pi}\phi_F \tag{4.108}$$

We can define the total charge and chiral sectors in terms of the right- and left-moving particle numbers Q_R and Q_L as:

$$Q_c = \frac{Q_R + Q_L}{2} \tag{4.109}$$

$$Q_x = \frac{Q_R - Q_L}{2} \tag{4.110}$$

Substituting into the excitation energy expression yields:

$$E_{-1} = \frac{v_F}{L}\left(\frac{1}{2\pi}\phi_F^2 + 2\pi\left[Q_c^2 + Q_x^2\right] + 2Q_x\phi_F\right) + \frac{2\pi v_F}{L}\sum_i N_i - \frac{\pi v_F}{6L} \tag{4.111}$$

To match with the microscopic expression, we expand E_n with explicit coefficients:

$$\frac{2\pi v_F}{L}E_n = \frac{2\pi v_F}{L}\left[m^2 + (n+\delta)^2 + N - \frac{1}{12}\right] \tag{4.112}$$

$$= \frac{2\pi v_F}{L}\left[m^2 + (n+\delta)^2\right] + \frac{2\pi v_F}{L}N - \frac{\pi v_F}{6L} \tag{4.113}$$

Comparing with Eq. (4.107), we identify:

$$N = \sum_i N_i \in \mathbb{N}_0 \tag{4.114}$$

doi:10.6342/NTU202501665

indicating that N represents the total level shift accumulated by promoting individual particles. As expected, this quantity is always non-negative.

For the m, n-dependent part of the BCFT energy spectrum, we identify the quantum numbers as:

$$m = Q_c \in \mathbb{Z} \tag{4.115}$$

$$n = Q_x \in \mathbb{Z} \tag{4.116}$$

The excitation number m, associated with the dual boson Y, corresponds to adding Q_c particles equally to both left- and right-moving sectors, representing a charge-sector excitation. In contrast, the excitation number n, associated with the boson X, corresponds to transferring Q_x particles from one sector to the other, characterizing a chiral excitation. This chiral transfer is precisely the process depicted in Fig. 4.8.

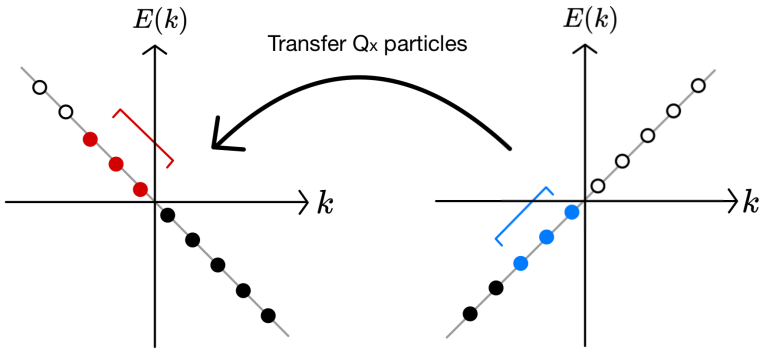

Figure 4.8: Transfer Q particles by removing Q particles from one sector and adding them to the other. The horizontal axis represents momentum k near the Fermi point k_F, while the vertical axis denotes the energy $E(k)$ near the Fermi energy E_F. Solid dots indicate occupied energy levels, and hollow dots represent unoccupied levels. Blue and red dots correspond to particle removal and addition, respectively.

and the full L^{-1} excitation energy simplifies to:

$$E_{-1} = \frac{2\pi v_F}{L} Q_c^2 + \frac{2\pi v_F}{L} \left(Q_x + \frac{1}{2\pi} \phi_F \right)^2 + \frac{2\pi v_F}{L} \sum_i N_i + \frac{\pi v_F}{6L} \tag{4.117}$$

doi:10.6342/NTU202501665

This expression now mirrors the BCFT formula energies:

$$\frac{2\pi v_F}{L}E_n = \frac{2\pi v_F}{L}\left(m^2 + (n+\delta)^2 + N - \frac{1}{12}\right)$$

demonstrating a precise match between the microscopic excitations and the BCFT structure.

A straightforward physical interpretation is that we raise n particles in one sector by n levels, leading to the n^2 contribution in energy. Subsequently, transferring these particles to the opposite sector introduces an additional phase shift, yielding the $2n\delta$ term. This two-step process gives rise to the full $(n+\delta)^2$ structure characteristic of BCFT energy levels.

Thus, we confirm that the excitation spectrum derived from the lattice system precisely matches the excited spectrum predicted by BCFT. It is worth emphasizing that this correspondence holds in both non-Hermitian and Hermitian impurity limits, demonstrating the robustness of the mapping.

Now, considering periodic boundary conditions, corresponding to integer values of ℓ, we find the excitation energy for adding or removing Q particles in either sector takes the form:

$$\Delta E_Q = \frac{v_F}{L}\left[2\pi\frac{Q(Q+1)}{2} \pm Q\phi_{\pm}(k_F^{\pm})\right], \quad Q \in \mathbb{Z} \tag{4.118}$$

This leads to the total L^{-1} correction to the energy:

$$E_{-1} = \frac{2\pi v_F}{L}Q_c(Q_c+1) + \frac{2\pi v_F}{L}\left(Q_x + \frac{1}{2\pi}\phi_F\right)^2 + \frac{2\pi v_F}{L}\sum_i N_i + \frac{\pi v_F}{6L} \tag{4.119}$$

This result exhibits a degeneracy in Q_c, as the total energy remains invariant under $Q_c = 0$

doi:10.6342/NTU202501665

(i.e., $Q_R = Q_L = 0$) or $Q_c = -1$ (i.e., $Q_R = Q_L = -1$). Physically, this reflects the freedom to occupy or remove the particle lying exactly at the Fermi level without changing the system' s total energy. Such even/odd or integer/half-integer structures in quantum numbers reflect the underlying conformal tower structure and closely resemble scenarios observed in the Kondo effect [38].

4.7 Physical Implications and Interpretation

We consider a tight-binding system with a single non-Hermitian defect, which naturally gives rise to a non-unitary scattering matrix (S-matrix), characteristic of open systems with gain or loss of probability. Via the folding trick, this setup can be mapped to a boundary conformal field theory, where the impurity term in the lattice model corresponds to a boundary term in the field theory. Both induce a shift in the ground state (critical) energy. Bosonization allows us to reformulate the system in terms of two bosonic fields with boundaries: one set by the defect and the other by the clean edge.

While the system initially appears to have central charge $c = 2$, a decomposition into even and odd combinations of the bosonic fields, denoted X and Y, simplifies the problem. Notably, the odd component Y decouples from the impurity and obeys a fixed boundary condition, leaving only the X-sector dynamically sensitive to the defect. As a result, the effective theory reduces to a single-component bosonic system with a tunable boundary condition. This reduction, however, demands care in reconstructing the full spectrum, as it relies on the gluing condition that ties the even and odd sectors together.

In this BCFT framework, a vanishing barrier corresponds to a Dirichlet boundary condition (perfect transmission), an infinitely strong barrier corresponds to a Neumann

doi:10.6342/NTU202501665

boundary condition (perfect reflection), and the free-fermion point marks a critical, exactly marginal perturbation that allows continuous interpolation between these two limits. This interpolation is encoded in the boundary S-matrix, where the transmission and reflection coefficients vary smoothly with the impurity strength.

Importantly, the unitarity of the S-matrix is directly linked to the Hermiticity of the microscopic defect: a Hermitian defect yields a unitary gluing condition in BCFT, while a non-Hermitian defect leads to non-unitary dynamics, often associated with amplification, attenuation, or more exotic phenomena. Yet, in certain regimes, such non-Hermitian systems can exhibit entirely real spectra, hinting at underlying pseudo-Hermitian or PT-symmetric structures that deserve deeper exploration.

doi:10.6342/NTU202501665

Chapter 5 Discussion and Conclusion

5.1 Summary of Major Results

We establish a correspondence between a non-Hermitian lattice system with a localized impurity and a boundary conformal field theory featuring a sine-Gordon-type boundary interaction. By applying the folding trick, the impurity is mapped onto a conformal boundary term, enabling a direct identification between the scattering matrix of the lattice model and the gluing matrix in the BCFT. The key correspondences are summarized in Table 5.1.

Non-Hermitian System	**Boundary CFT**
Impurity strength $v, \bar{v}$	Boundary couplings $g, \bar{g}$
Scattering matrix S	Gluing matrix U
$SL(2,\mathbb{C})$	$SL(2,\mathbb{C})$
Defect-free	Dirichlet boundary condition
Decoupled/infinite barrier	Neumann boundary condition
Hermiticity	Unitarity
Ground state energy E_c	Ground state energy E_0
Energy shift ϕ_F	Energy shift δ
Excited levels number N_i	Excitation number $N \in \mathbb{N}_0$
Extra particle number Q_c	Excitation number $m \in \mathbb{Z}$
Particle difference number Q_x	Excitation number $n \in \mathbb{Z}$

Table 5.1: Correspondence between non-Hermitian lattice systems and boundary conformal field theory

While the impurity strength in the lattice model maps onto the boundary coupling in BCFT, the Hermiticity condition corresponds precisely to the unitarity of the gluing ma-

doi:10.6342/NTU202501665

trix. This correspondence reveals a deeper structural insight: whereas the non-Hermitian model permits probability gain or loss through complex couplings, the conformal field theory encodes such non-conservation as deviations from unitary boundary conditions.

Furthermore, at the Fermi point (e.g., $k = \pi/2$), we observe that the impurity-induced energy shift, including both ground state and excited states, in the lattice model, has a direct analogue in the finite-size corrections to the BCFT energy spectrum. Notably, the charge-like excitation number corresponds to excitation modes of the decoupled Y-boson sector, while the chiral-like excitation number maps to excitation modes of the interacting X-boson sector.

This correspondence provides a unified framework for characterizing open quantum systems with gain and loss through conformal boundary data, offering novel insights into the critical behavior of non-Hermitian systems from a BCFT perspective. It opens new avenues for analyzing non-Hermitian quantum dynamics using the well-established tools of boundary CFT, with potential applications to quantum impurity problems, open quantum systems, and condensed matter platforms that exhibit non-Hermitian effects.

5.2 Potential Future Directions

Looking ahead, a natural next step is to numerically validate our analytical results. In particular, having simulation data for comparison. We also aim to extend our analysis to other physical observables, including boundary entropy, boundary correlation functions, and the identification of leading irrelevant operators.

On the theoretical side, we plan to apply bosonization techniques to study systems with interactions, spin degrees of freedom, and mass terms. These generalizations could

doi:10.6342/NTU202501665

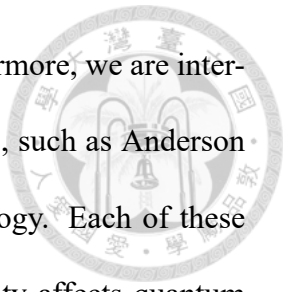

reveal new aspects of boundary dynamics and phase behavior. Furthermore, we are interested in exploring broader phenomena within non-Hermitian systems, such as Anderson localization, RG flow structures, exceptional points, and band topology. Each of these directions has the potential to shed new light on how non-Hermiticity affects quantum criticality and boundary physics. Collectively, these investigations offer a promising path toward a deeper understanding of non-Hermitian quantum systems, their boundary behavior, and their potential for realization in precisely controlled experimental platforms.

5.3 Concluding Remarks

Our analysis reveals that key BCFT concepts, such as gluing matrices, emerge naturally in the study of non-unitary dynamics and provide powerful tools for understanding non-Hermitian physics. While the present results are primarily theoretical, they lay the foundation for future numerical and experimental investigations. We anticipate that such efforts will help bridge discrete lattice models with quantum field theory insights in increasingly realistic settings. Finally, we hope that this work not only stimulates further theoretical developments but also informs experimental exploration across a broad range of non-Hermitian platforms.

doi:10.6342/NTU202501665

doi:10.6342/NTU202501665

References

[1] Kazuaki Takasan, Masaki Oshikawa, and Haruki Watanabe. Adiabatic transport in one-dimensional systems with a single defect, 2021.

[2] Kazuaki Takasan, Masaki Oshikawa, and Haruki Watanabe. Drude weights in one-dimensional systems with a single defect. Physical Review B, 107(7), February 2023.

[3] Yuto Ashida, Zongping Gong, and Masahito Ueda. Non-hermitian physics. Advances in Physics, 69(3):249–435, 2020.

[4] Paul Ginsparg. Applied conformal field theory. arXiv preprint hep-th/9108028, 1988.

[5] Philippe Francesco, Pierre Mathieu, and David Sénéchal. Conformal field theory. Springer Science & Business Media, 2012.

[6] Ralph Blumenhagen and Erik Plauschinn. Introduction to conformal field theory: with applications to String theory, volume 779. Springer Science & Business Media, 2009.

[7] Curtis G. Callan, Igor R. Klebanov, Andreas W.W. Ludwig, and Juan M. Maldacena.

doi:10.6342/NTU202501665

Exact solution of a boundary conformal field theory. Nuclear Physics B, 422(3):417–448, July 1994.

[8] Joseph Polchinski and Lárus Thorlacius. Free fermion representation of a boundary conformal field theory. Physical Review D, 50(2):R622–R626, July 1994.

[9] M. Hasselfield, Taejin Lee, G.W. Semenoff, and P.C.E. Stamp. Critical boundary sine-gordon revisited. Annals of Physics, 321(12):2849–2875, December 2006.

[10] Carl M. Bender and Stefan Boettcher. Real spectra in non-hermitian hamiltonians having pt symmetry. Physical Review Letters, 80(24):5243–5246, 1998.

[11] Carl M. Bender. Making sense of non-hermitian hamiltonians. Reports on Progress in Physics, 70(6):947–1018, 2007.

[12] Stefan Banach. Theory of linear operations, volume 38. Elsevier, 1987.

[13] Emil J. Bergholtz, Jan Carl Budich, and Flore K. Kunst. Exceptional topology of non-hermitian systems. Reviews of Modern Physics, 93(1):015005, 2021.

[14] Ali Mostafazadeh. Pseudo-hermitian description of pt-symmetric systems defined on a complex contour. Journal of Physics A: Mathematical and General, 38(14):3213, 2005.

[15] Ali Mostafazadeh. Pseudo-hermiticity versus pt symmetry: The necessary condition for the reality of the spectrum of a non-hermitian hamiltonian. Journal of Mathematical Physics, 43(1):205–214, 2002.

[16] Ali Mostafazadeh. Pseudo-hermiticity versus pt-symmetry. ii. a complete characterization of non-hermitian hamiltonians with a real spectrum. Journal of Mathematical Physics, 43(5):2814–2816, May 2002.

doi:10.6342/NTU202501665

[17] Liang Feng, Ramy El-Ganainy, and Li Ge. Non-hermitian photonics based on parity–time symmetry. Nature Photonics, 11:752–762, 2017.

[18] Mohammad-Ali Miri and Andrea Alù. Exceptional points in optics and photonics. Science, 363(6422):eaar7709, 2019.

[19] Şahin K. Özdemir, Stefan Rotter, Franco Nori, and Lan Yang. Parity–time symmetry and exceptional points in photonics. Nature Materials, 18(8):783–798, 2019.

[20] Yi-Cheng Wang, Jhih-Shih You, and Hsiang-Hua Jen. A non-hermitian optical atomic mirror. Nature Communications, 13(1):4598, 2022.

[21] C. E. Rüter, K. G. Makris, R. El-Ganainy, D. N. Christodoulides, M. Segev, and D. Kip. Observation of parity–time symmetry in optics. Nature Physics, 6:192–195, 2010.

[22] W. Chen, Ş. K. Özdemir, G. Zhao, J. Wiersig, and L. Yang. Exceptional points enhance sensing in an optical microcavity. Nature, 548:192–196, 2017.

[23] Z. Gong, Y. Ashida, K. Kawabata, K. Takasan, S. Higashikawa, and M. Ueda. Topological phases of non-hermitian systems. Physical Review X, 8:031079, 2018.

[24] S. Yao and Z. Wang. Edge states and topological invariants of non-hermitian systems. Physical Review Letters, 121:086803, 2018.

[25] Z. Li, L.-W. Wang, X. Wang, Z.-K. Lin, G. Ma, and J.-H. Jiang. Observation of dynamic non-hermitian skin effects. Nature Communications, 15:6544, 2024.

[26] Romain Couvreur, Jesper Lykke Jacobsen, and Hubert Saleur. Entanglement in nonunitary quantum critical spin chains. Physical review letters, 119(4):040601, 2017.

doi:10.6342/NTU202501665

[27] Po-Yao Chang, Jhih-Shih You, Xueda Wen, and Shinsei Ryu. Entanglement spectrum and entropy in topological non-hermitian systems and nonunitary conformal field theory. Physical Review Research, 2(3), July 2020.

[28] Michael H Freedman, Jan Gukelberger, Matthew B Hastings, Simon Trebst, Matthias Troyer, and Zhenghan Wang. Galois conjugates of topological phases. Physical Review B—Condensed Matter and Materials Physics, 85(4):045414, 2012.

[29] Laurens Lootens, Robijn Vanhove, Jutho Haegeman, and Frank Verstraete. Galois conjugated tensor fusion categories and nonunitary conformal field theory. Physical review letters, 124(12):120601, 2020.

[30] Sora Cho and Matthew P. A. Fisher. Criticality in the two-dimensional random-bond ising model. Phys. Rev. B, 55:1025–1031, Jan 1997.

[31] Masaki Oshikawa and Ian Affleck. Boundary conformal field theory approach to the critical two-dimensional ising model with a defect line. Nuclear Physics B, 495(3):533–582, 1997.

[32] Gregory Moore and Nicholas Read. Nonabelions in the fractional quantum hall effect. Nuclear Physics B, 360(2-3):362–396, 1991.

[33] Thors Hans Hansson, Maria Hermanns, Steven H Simon, and Susanne F Viefers. Quantum hall physics: Hierarchies and conformal field theory techniques. Reviews of Modern Physics, 89(2):025005, 2017.

[34] Ian Affleck and Andreas WW Ludwig. The kondo effect, conformal field theory and fusion rules. Nuclear Physics B, 352(3):849–862, 1991.

[35] Ian Affleck, Andreas WW Ludwig, H-B Pang, and DL Cox. Relevance of anisotropy

doi:10.6342/NTU202501665

in the multichannel kondo effect: Comparison of conformal field theory and numerical renormalization-group results. Physical Review B, 45(14):7918, 1992.

[36] Ian Affleck and Andreas WW Ludwig. Exact conformal-field-theory results on the multichannel kondo effect: Single-fermion green's function, self-energy, and resistivity. Physical Review B, 48(10):7297, 1993.

[37] Andreas W.W. Ludwig and Ian Affleck. Exact conformal-field-theory results on the multi-channel kondo effect: Asymptotic three-dimensional space- and time-dependent multi-point and many-particle green's functions. Nuclear Physics B, 428(3):545–611, 1994.

[38] Ian Affleck. Conformal field theory approach to the kondo effect. arXiv preprint cond-mat/9512099, 1995.

[39] C. L. Kane and Matthew P. A. Fisher. Transport in a one-channel luttinger liquid. Phys. Rev. Lett., 68:1220–1223, Feb 1992.

[40] C. L. Kane and Matthew P. A. Fisher. Transmission through barriers and resonant tunneling in an interacting one-dimensional electron gas. Phys. Rev. B, 46:15233–15262, Dec 1992.

doi:10.6342/NTU202501665

doi:10.6342/NTU202501665

Appendix A — Virasoro algebra

A.1 The Witt Algebra

The Witt algebra is a fundamentally important infinite-dimensional Lie algebra in mathematics and theoretical physics, particularly in the contexts of conformal field theory (CFT). It serves as the underlying structure of the Virasoro algebra, which is obtained from the Witt algebra by introducing a central extension. The Witt algebra is typically defined as the infinite-dimensional Lie algebra of infinitesimal diffeomorphisms on the circle. Its generators satisfy the following relations:

$$\begin{aligned} l_n &\equiv -z^{n+1}\partial_z \\ \bar{l}_n &\equiv -\bar{z}^{n+1}\partial_{\bar{z}} \qquad n \in \mathbb{Z} \end{aligned} \tag{A.1}$$

and their commutation relation:

$$\begin{aligned} [l_m, l_n] &= z^{m+1}\partial_z\left(z^{n+1}\partial_z\right) - z^{n+1}\partial_z\left(z^{m+1}\partial_z\right) \\ &= (m-n)z^{m+n+1}\partial_z \\ &= (m-n)l_{m+n} \end{aligned} \tag{A.2}$$

similarly,

$$[\bar{l}_m, \bar{l}_n] = (m-n)\bar{l}_{m+n} \tag{A.3}$$

doi:10.6342/NTU202501665

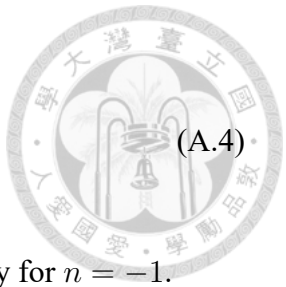

also,

$$[l_m, \bar{l}_n] = 0 \tag{A.4}$$

note that the operator $l_n = -z^{n+1}\partial_z$ is non-singular at $z = 0$ only for $n = -1$.

Globally defined conformal transform on Riemann sphere: $\mathbb{S}^2 = \mathbb{C} \cup \{\infty\}$ generated by $\{l_{-1}, l_0, l_1\}$:

$$z \mapsto \frac{az + b}{cz + d} \tag{A.5}$$

which is the Möbius group $\mathrm{SL}(2, \mathbb{C})/\mathbb{Z}_2$

A.2 Central Extension

Consider the central extension $\hat{\mathfrak{g}} = \mathfrak{g} \oplus \mathbb{C}$ of a Lie algebra $\mathfrak{g}$ by $\mathbb{C}$.

Define the Lie bracket on $\hat{\mathfrak{g}}$ as follows:

$$\begin{aligned} [\tilde{x}, \tilde{y}]_{\hat{\mathfrak{g}}} &= [x, y]_{\mathfrak{g}} + c \cdot p(x, y) \\ [\tilde{x}, c]_{\hat{\mathfrak{g}}} &= 0 \\ [c, c]_{\hat{\mathfrak{g}}} &= 0 \end{aligned} \tag{A.6}$$

for $\tilde{x}, \tilde{y} \in \hat{\mathfrak{g}}$, $x, y \in \mathfrak{g}$, $c \in \mathbb{C}$.

where $p : \mathfrak{g} \times \mathfrak{g} \to \mathbb{C}$ is a bilinear map.

When including the central extension, the Witt algebra becomes the Virasoro algebra. Its generators are also usually denoted by L_n, but with an additional central element c (the

doi:10.6342/NTU202501665

central charge). The commutation relations then become:

$$[L_m, L_n] = (m-n)L_{m+n} + \frac{c}{12}(m^3 - m)\delta_{m+n,0}, \quad [L_n, c] = 0 \tag{A.7}$$

Here, c is a central known as the central charge.

In two-dimensional conformal field theory (2D CFT), the central charge c is an essential and fundamental parameter. It not only dictates the mathematical structure of the conformal field theory by characterizing the central extension term of the Virasoro algebra, but also profoundly influences the theory's physical interpretation. Mathematically, the central charge represents the nontrivial central extension of the Virasoro algebra, signifying an intrinsic algebraic anomaly. Physically, it serves as a measure of the number of degrees of freedom within the theory and is intimately connected to conformal anomalies and renormalization group (RG) flows. Consequently, the central charge provides deep insights into the critical phenomena and dynamic behaviors of theories as they evolve from ultraviolet (UV) to infrared (IR) regimes.

A.3 Correlation Functions and Operator Product Expansion (OPE)

The fundamental OPE of the holomorphic energy-momentum tensor in two-dimensional CFT is:

$$T(z)T(w) = \frac{c}{2}\frac{1}{(z-w)^4} + \frac{2T(w)}{(z-w)^2} + \frac{\partial T(w)}{(z-w)} + \cdots \tag{A.8}$$

doi:10.6342/NTU202501665

This OPE follows from the Laurent expansion of $T(z)$ in radial quantization:

$$T(z) = \sum_{n\in\mathbb{Z}} z^{-n-2} L_n, \quad \text{where } L_n = \frac{1}{2\pi i}\oint dz\, z^{n+1} T(z) \tag{A.9}$$

By definition, the OPE between $T(z)$ and a primary field $\phi(w,\bar{w})$ of conformal weight is:

$$T(z)\phi(w,\bar{w}) = \frac{h}{(z-w)^2}\phi(w,\bar{w}) + \frac{1}{(z-w)}\partial\phi(w,\bar{w}) + \cdots \tag{A.10}$$

The holomorphic part is equivalent to the commutation relation:

$$[L_m, \phi_n] = (h-1)\, m\delta_{m+n} - n\phi_{m+n} \qquad \forall m,n \in \mathbb{Z} \tag{A.11}$$

If a field transforms covariantly under the global conformal generators L_{-1}, L_0, L^1 but not under the full Virasoro algebra, it is referred to as a quasi-primary field.

In a conformal field theory, the form of correlation functions is highly constrained. For holomorphic primary fields, the 2-point and 3-point functions take the form:

$$\langle \phi_i(z)\phi_j(w)\rangle = \frac{\delta_{ij}}{(z-w)^{2h_i}} \tag{A.12}$$

$$\langle \phi_1(z_1)\phi_2(z_2)\phi_3(z_3)\rangle = \frac{C_{123}}{z_{12}^{h_1+h_2-h_3}\, z_{23}^{h_2+h_3-h_1}\, z_{31}^{h_3+h_1-h_2}} \tag{A.13}$$

where $z_{ij} = z_i - z_j$. Where δ_{ij} and C_{123} is known as structure constant.

doi:10.6342/NTU202501665

Consider:

$$\phi_i(z)\phi_j(w) = \sum_{k,n\geq 0} C_{ij}^k \, a_{ijk}^n \, \frac{1}{(z-w)^{h_i+h_j-h_k-n}} \, \frac{1}{n!}\partial^n \phi_k(w) \tag{A.14}$$

Take $w = 1$, then consider the 3-point function:

$$\langle(\phi_i(z)\phi_j(1))\phi_k(0)\rangle = \sum_{n\geq 0} C_{ij}^k \, a_{ijk}^n \, \frac{1}{(z-1)^{h_i+h_j-h_k-n}} \, \frac{1}{n!} \, \langle \partial^n \phi_k(1)\phi_k(0)\rangle \tag{A.15}$$

Using the 2-point function:

$$\langle \partial_z^n \phi_k(z)\phi_k(0)\rangle = \partial_z^n \left(\frac{d_{kk}\,\delta_{hk,hk}}{z^{2h_k}}\right) = (-1)^n \frac{(2h_k+n-1)!}{n!(2h_k-1)!} \frac{d_{kk}\,\delta_{hk,hk}}{z^{2h_k+n}} \tag{A.16}$$

So we obtain:

$$\langle \phi_i(z)\phi_j(1)\phi_k(0)\rangle = \sum_{n\geq 0} C_{ij}^k \, d_{kk} \, a_{ijk}^n \cdot \frac{(2h_k+n-1)!}{n!(2h_k-1)!} \cdot \frac{1}{(z-1)^{h_i+h_j-h_k-n}} \cdot \frac{(-1)^n}{(z-1)^{2h_k+n}} \tag{A.17}$$

Combine the powers of $(z-1)$, we get:

$$\langle \phi_i(z)\phi_j(1)\phi_k(0)\rangle = \frac{C_{ijk}}{(z-1)^{h_i+h_j-h_k} z^{h_k+h_i-h_j}(1-z)^{h_j+h_k-h_i}} \tag{A.18}$$

Let $x \equiv z-1$, $H \equiv h_i + h_j - h_k$, and expand:

$$\frac{C_{ijk}}{(1+x)^H} = C_{ijk} \sum_{n=0}^{\infty} \binom{H+n-1}{n} (-1)^n x^n \tag{A.19}$$

doi:10.6342/NTU202501665

Compare coefficients of x^n, we get:

$$a_{ijk}^n = \frac{(2h_k+n-1)!}{n!(2h_k-1)!} \cdot \frac{1}{(H+n-1)!} \tag{A.20}$$

$$C_{ijk} = C_{ij}^k d_{kk} \tag{A.21}$$

To extract commutation relations, we can use the Laurent mode expansion:

$$\phi_i(z) = \sum_n \phi_{i,n}\, z^{-n-h_i} \tag{A.22}$$

We have:

$$[\phi_{i,m}, \phi_{j,n}] = \sum_k L_i^k\, \mathcal{P}_{ijk}(m,n)\, \phi_{k,m+n} + d_{ij}\, \delta_{m+n}\, \frac{(m+h_i-1)!}{(h_i-1)!} \tag{A.23}$$

where

$$\mathcal{P}_{ijk}(m,n) = \sum_{r+s=t} C_{rs}^{ijk} \cdot (-m+h_i-1)_r \cdot (-n+h_j-1)_s, \quad r+s = h_i+h_j-h_k-1 \tag{A.24}$$

and

$$C_{rs}^{ijk} = (-1)^r \cdot \frac{(2h_k-1)!}{(h_i+h_j+h_k-2)!} \cdot \prod_{t=0}^{s-1}(h_j+h_k-2-t) \cdot \prod_{u=0}^{r-1}(h_i+h_k-2-u) \tag{A.25}$$

With these coefficients, we can re-discover the Virasoro algebra:

$$[L_m, L_n] = \mathcal{C}_{LL} \cdot \mathcal{P}_{LLL}(m,n)\, L_{m+n} + d_{LL}\, \delta_{m+n}\, \frac{m(m^2-1)}{6} \tag{A.26}$$

doi:10.6342/NTU202501665

Since $h = 2$ for $T(z)$, we compute:

$$\mathcal{P}_{LLL}(m,n) = C_{1,0}^{LLL}(-m+1) + C_{0,1}^{LLL}(-n+1) \tag{A.27}$$

$$C_{1,0}^{LLL} = (-1)^1 \cdot \frac{3!}{4!} \cdot 2 = -\frac{1}{2} \tag{A.28}$$

$$C_{0,1}^{LLL} = (+1) \cdot \frac{3!}{4!} \cdot 2 = +\frac{1}{2} \tag{A.29}$$

So we get:

$$[L_m, L_n] = \mathcal{C}_{LL} \cdot \frac{m-n}{2} L_{m+n} + d_{LL}\, \delta_{m+n}\, \frac{m^3 - m}{6} \tag{A.30}$$

Compare with standard Virasoro result, we fix:

$$\mathcal{C}_{LL} = 2, \qquad d_{LL} = \frac{c}{2} \tag{A.31}$$

When considering the operator product expansion (OPE) of primary fields in conformal field theory (CFT), we expand them in terms of a complete basis of derivative fields accompanied by corresponding expansion coefficients. By carefully comparing these expansions with the explicit forms of two- and three-point correlation functions, one can rigorously derive the general form of these expansion coefficients. Furthermore, by decomposing primary fields into their mode expansions and analyzing the commutators between these mode operators, it becomes clear that their commutation relations naturally split into two distinct parts. The first part arises directly from the three-point structure constants and their derivative terms, while the second, additional contribution, the central term, is generated as a consequence of the regularization procedure of the field operators. Through this systematic process, the structure of the Virasoro algebra is explicitly recon-

doi:10.6342/NTU202501665

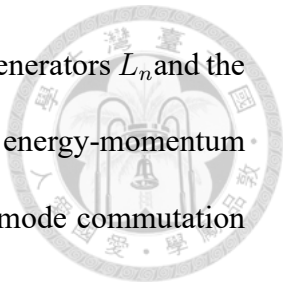

structed, revealing both the Lie algebra commutation relations of the generators L_n and the associated central extension term. In particular, when focusing on the energy-momentum tensor $T(z)$ of conformal weight $h = 2$, a precise calculation of the mode commutation relations yields:

$$[L_m, L_n] = (m-n)L_{m+n} + \frac{c}{12}m(m^2-1)\delta_{m+n,0}, \tag{A.32}$$

which precisely matches the definition of the Virasoro algebra with central charge c. Thus, through this derivation, we not only recover the Virasoro algebra itself but also gain a clear understanding of the central extension' s origin as emerging from the regularization and renormalization inherent in the mode expansion of the operator product expansion.

doi:10.6342/NTU202501665

Appendix B — Unitarity Check of Gluing Matrix

We now examine the conditions under which the gluing matrix U, acting on the boundary fermions, remains unitary. Recall the parametrized form of U, introduced in Eq. 3.37:

$$U = \begin{pmatrix} e^{-2\pi iA}\sqrt{1-\pi^2 g\bar{g}} & -i\pi g \\ -i\pi\bar{g} & e^{2\pi iA}\sqrt{1-\pi^2 g\bar{g}} \end{pmatrix}.$$

To ensure physical consistency and probability conservation at the boundary, we require that $U \in U(2)$, i.e.,

$$UU^\dagger = \mathbb{I}. \tag{B.33}$$

We compute this product explicitly:

$$UU^\dagger = \begin{pmatrix} e^{-2\pi iA}\sqrt{1-\pi^2 g\bar{g}} & -i\pi g \\ -i\pi\bar{g} & e^{2\pi iA}\sqrt{1-\pi^2 g\bar{g}} \end{pmatrix} \begin{pmatrix} e^{2\pi iA^*}\sqrt{1-\pi^2 g\bar{g}}^* & i\pi\bar{g}^* \\ i\pi g^* & e^{-2\pi iA^*}\sqrt{1-\pi^2 g\bar{g}}^* \end{pmatrix} \tag{B.34}$$

doi:10.6342/NTU202501665

The components are:

$$(UU^\dagger)_{11} = e^{-2\pi iA}\sqrt{1-\pi^2 g\bar{g}}\cdot e^{2\pi iA^*}\sqrt{1-\pi^2 g\bar{g}}^* + (-i\pi g)(i\pi g^*)$$
$$= e^{-2\pi i(A-A^*)}|\sqrt{1-\pi^2 g\bar{g}}|^2 + \pi^2|g|^2, \tag{B.35}$$

$$(UU^\dagger)_{12} = (i\pi\bar{g}^*)\cdot e^{-2\pi iA}\sqrt{1-\pi^2 g\bar{g}} + (-i\pi g)\cdot e^{-2\pi iA^*}\sqrt{1-\pi^2 g\bar{g}}^*, \tag{B.36}$$

$$(UU^\dagger)_{21} = (i\pi g^*)\cdot e^{2\pi iA}\sqrt{1-\pi^2 g\bar{g}} + (-i\pi\bar{g})\cdot e^{2\pi iA^*}\sqrt{1-\pi^2 g\bar{g}}^*, \tag{B.37}$$

$$(UU^\dagger)_{22} = e^{2\pi iA}\sqrt{1-\pi^2 g\bar{g}}\cdot e^{-2\pi iA^*}\sqrt{1-\pi^2 g\bar{g}}^* + (-i\pi\bar{g})(i\pi\bar{g}^*)$$
$$= e^{2\pi i(A-A^*)}|\sqrt{1-\pi^2 g\bar{g}}|^2 + \pi^2|\bar{g}|^2. \tag{B.38}$$

In our consideration, $A \in \mathbb{R}$. To make $UU^\dagger = \mathbb{I}$, we can find the unitarity conditions:

$$\bar{g} = g^*, \quad |g| \leq \frac{1}{\pi}$$

doi:10.6342/NTU202501665

Appendix C — Expansion and Correction of q_n

We consider the quantization condition

$$q_n = k_n + \frac{1}{L}\phi(q_n), \quad \text{where} \quad k_n = \frac{2\pi n}{L}, \quad n \in \mathbb{Z} \tag{C.39}$$

and $\phi(k)$ is a smooth phase shift function associated with scattering or boundary effects. Our goal is to systematically expand q_n in powers of $1/L$, which is particularly useful in large-L asymptotic analysis.

We postulate an expansion of the form

$$q_n = k_n + \frac{a_n}{L} + \frac{b_n}{L^2} + \mathcal{O}\left(\frac{1}{L^3}\right) \tag{C.40}$$

where a_n and b_n are to be determined order-by-order in $1/L$. Substituting into the original quantization condition yields:

$$k_n + \frac{a_n}{L} + \frac{b_n}{L^2} + \cdots = k_n + \frac{1}{L}\phi\left(k_n + \frac{a_n}{L} + \frac{b_n}{L^2} + \cdots\right) \tag{C.41}$$

doi:10.6342/NTU202501665

Canceling k_n from both sides and expanding ϕ around k_n, we obtain:

$$\frac{a_n}{L} + \frac{b_n}{L^2} + \cdots = \frac{1}{L}\left[\phi(k_n) + \phi'(k_n)\left(\frac{a_n}{L} + \frac{b_n}{L^2}\right) + \frac{1}{2}\phi''(k_n)\left(\frac{a_n}{L}\right)^2 + \cdots\right] \tag{C.42}$$

Matching terms order-by-order in $1/L$, we find:

- **First order** $(\mathcal{O}(1/L))$:

$$a_n = \phi(k_n)$$

- **Second order** $(\mathcal{O}(1/L^2))$:

$$b_n = \phi'(k_n)\phi(k_n)$$

Combining these, the expansion of q_n up to second order is:

$$q_n = k_n + \frac{1}{L}\phi(k_n) + \frac{1}{L^2}\phi'(k_n)\phi(k_n) + \mathcal{O}\left(\frac{1}{L^3}\right) \tag{C.43}$$

This expression captures the leading and subleading finite-size corrections to the quantized momenta q_n, and can be directly used in evaluating quantities such as energy spectra, density of states, and finite-size corrections to thermodynamic observables.

doi:10.6342/NTU202501665